IEEE Open Journal of
Intelligent Transportation
Systems

Received 16 May 2023; revised 30 June 2023, 18 August 2023, and 21 September 2023; accepted 12 October 2023. Date of publication 18 October 2023; date of current version 7 November 2023.

Digital Object Identifier 10.1109/OJITS.2023.3325257

Bandwidth-Based Traffic Signal Coordination Models for Split or Mixed Phasing Schemes in Various Types of Networks

BINBIN JING[1], QUAN SHI[1], CONG HUANG[1], PENG PING[1], AND YONGJIE LIN[2] (Member, IEEE)

[1]School of Transportation and Civil Engineering, Nantong University, Nantong 226019, China

[2]School of Civil Engineering and Transportation, South China University of Technology, Guangzhou 510641, China

CORRESPONDING AUTHOR: P. PING (e-mail: pingpeng@ntu.edu.cn)

This work was supported in part by the National Natural Science Foundation of China under Grant 52102395, and in part by the Natural Science Foundation of the Jiangsu Higher Education Institutions of China under Grant 21KJB580016.

ABSTRACT Bandwidth-based traffic signal coordination has long been an effective technique to make traffic flows within a network more efficient, smoother, and safer. Existing network bandwidth optimization models mainly focus on maximizing the bandwidth under NEMA phasing. The network bandwidth maximization under other typical phasing schemes, namely the split or mixed phasing, has not been intensively studied. To address this, a group of bandwidth-based network traffic signal coordination models is proposed for different types of traffic networks. All the proposed models can simultaneously optimize the key signal control variables, namely the phase sequences, offsets, and common cycle times. Additionally, all the developed models are formulated as mixed-integer linear programming problems, which guarantees that the global optimal solutions can be obtained using the branch-and-bound algorithm. The results of the presented index, which is defined as the absolute difference of the interference variables obtained through theoretical solutions and time–space diagrams, indicate that all the proposed models are correct. Furthermore, simulation results demonstrate that split phasing can significantly reduce the average delay time and the average number of stops compared with the existing NEMA phasing.

INDEX TERMS Bandwidth maximization, traffic signal coordination, phasing scheme, traffic network.

I. INTRODUCTION

CURRENTLY, traffic congestion has become one of the most serious problems faced by transportation authorities. Compared with costly and time-consuming measures, such as building new road infrastructures or expanding existing ones, efficient traffic signal control has been proven to be one of the most cost-effective ways to mitigate traffic congestion. Consequently, traffic signal optimization has been studied extensively over the past several decades. Research on traffic signal optimization can be roughly classified into three categories: classical mathematical methods, simulation-based methods, and artificial intelligence-based methods. The first category mainly focuses on developing relationships between indicators and signal parameters and then minimizing disutility indicators (e.g., delays [1], [2] and ecological cost [3]) or maximizing positive indicators (e.g., bandwidths [4], [5] and capacity [6]) using classical mathematical modeling. In the second category, TRANSYT [7] and TRANSYT-7F [8] are the frequently used simulation-based traffic signal timing optimization programs. Artificial intelligence methods represented by machine learning have been widely used in the field of transportation, such as traffic safety-related prediction [9], [10], traffic state prediction [11], [12], automated driving [13], [14], and traffic signal control [15], [16], [17]. References [15], [16], and [17] report the use of deep reinforcement learning to estimate the optimal traffic signal timing plans, which can be classified into the third category. These three types of methods can greatly improve the operational efficiency of the traffic streams. Due to the lower input requirements and

The review of this article was arranged by Associate Editor Yajie Zou.

the easier visualization of the coordination control effect, the bandwidth-based methods are the preferred choice of traffic engineers [18]. Therefore, this paper also focuses on bandwidth-based methods.

Morgan and Little [19] are pioneers that developed a model to coordinate arterial traffic signals for maximum bandwidth with fixed common cycle lengths, green and red times, and vehicle speeds. Soon afterward, significant improvements to this approach, e.g., allowing the common cycle lengths and vehicle speeds to vary within upper and lower limits, were made by Little [20]. Later, Little et al. [4] proposed the well-known MAXBAND model, which maximizes the two-way bandwidths along an arterial by concurrently modifying signal control variables such as the common cycle lengths, offsets, left-turn phase sequences, and progression speed. Based on MAXBAND, Chang et al. [21] developed the MAXBAND-86 model, which solved the signal synchronization problems in multiarterial closed networks. The bandwidths for each directional link yielded by MAXBAND are uniform. That is, MAXBNAD does not take into consideration the heterogeneity of each directional link. Different links have different demands for bandwidths, as the traffic volume and saturation flow rate on each link are not constant. Therefore, it is preferable that bandwidths vary with the links instead of being uniform along the entire arterial. To tackle this issue, Gartner et al. [5] proposed MULTIBAND, which yielded a variable bandwidth for each directional arterial link. Later, Stamatiadis and Gartner [22] extended MULTIBAND and developed a network version model named MULTIBAND-96. After that, a heuristic network decomposition procedure was presented by Gartner and Stamatiadis [23] for a fast solution to network bandwidth optimization problems. Following the logic of MAXBAND or MULTIBAND, researchers have further studied bandwidth optimization problems in recent years. Typical research on bandwidth optimization is summarized as follows. Zhang et al. [24] developed an asymmetric multi-band model named AM-Band, which can relax the symmetric band requirement of MULTIBAND. Yang et al. [25] proposed a multi-path model that provided bandwidths for multiple arterial path flows. Arsava et al. [26] proposed the OD-BAND model, which provided progression bands for arterial origin-destination (OD) streams. Ma et al. [18] presented a partition-enabled multi-mode model that provided progressive bands for both passenger cars and transit vehicles along a long arterial. Jing et al. [27] proposed a bandwidth optimization model, called Pband, which concurrently optimized the phasing scheme choices, phase sequences, and offsets. Zhang et al. [28] developed two bandwidth maximization models, MaxBandLA and MaxBandGN, which solved the signal coordination problems for long arterials and grid networks, respectively. Lu et al. [29] proposed an algebraic method for arterial green wave coordination control, which is applicable for mixed phasing schemes. Later, Lu et al. [30] extended the previous work [29] and presented an algebraic method for network-level green wave coordination control. Yan et al. [31] developed a network bandwidth optimization model to provide progressive bands for major traffic streams by using vehicle trajectory data. To enlarge the feasible region, Wang and Yao [32] proposed a network band model with permitting the relaxation of constraints.

In summary, arterial bandwidth optimization can improve the traffic flow efficiency on the main arterial, but that on the crossing arterials may be reduced. Network bandwidth optimization can coordinate traffic signals of all arterials within a network, which is more conducive to the improvement of the overall network efficiency than single arterial bandwidth optimization. However, existing bandwidth-based network traffic signal coordination models, represented by the well-recognized MAXBAND-86 or MULTIBAND-96, mainly maximize the bandwidth under NEMA phasing scheme. Network bandwidth maximization under the split or mixed phasing schemes (see Section II) has been not intensively studied. As a typical phasing scheme design mode at a signalized intersection, the split phasing has its own advantages. First, the split phasing can effectively balance the volume to capacity ratio, queue length and delay time of each lane [33]. Second, an intersection with through-left shared lanes can only operate with the split phasing instead of the NEMA phasing. Third, the split phasing can provide a wide phase sequence optimization space, which helps to obtain better traffic control effects. Therefore, it is very necessary to formulate new models to maximize the network bandwidth under the split or mixed phasing schemes. This paper proposes a group of models for different types of traffic networks to address the network bandwidth optimization problems under split and mixed phasing schemes.

The remainder of this paper is organized as follows. Section II describes the key concepts employed in this paper. In Section III, explanations of the problems is presented. In Section IV, the proposed network bandwidth optimization models are formulated. A numerical example is given in Section V to demonstrate the correctness and the superior performances of the proposed models. Conclusions are provided in the last section.

II. CONCEPTS

To facilitate the understanding of the proposed bandwidth-oriented models, some key concepts are introduced as below.

A. PHASING SCHEMES

1) *NEMA Phasing:* The NEMA phasing is a type of signal phasing scheme supported by the National Electrical Manufacturers Association (NEMA). Fig. 1(a) and (b) illustrate four possible kinds of phase sequences in the W-E and S-N directions of an intersection that operates with the NEMA phasing.

2) *Split Phasing:* The split phasing is a type of signal phasing scheme which traffic movements in each approach of an intersection receive the right-of-way in turn. Fig. 2 illustrates six possible kinds of phase sequences when the split

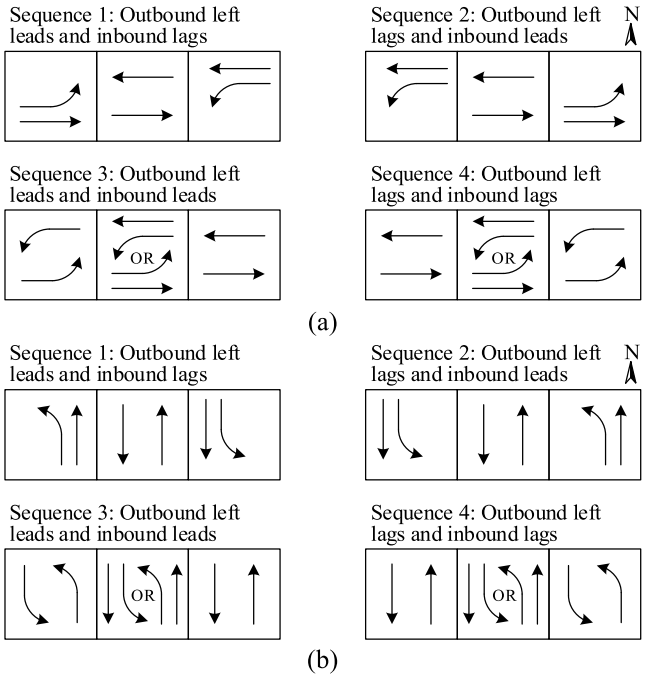

FIGURE 1. Four possible kinds of phase sequences in NEMA phasing scheme. (a) Phase sequences in the W-E direction. (b) Phase sequences in the S-N direction.

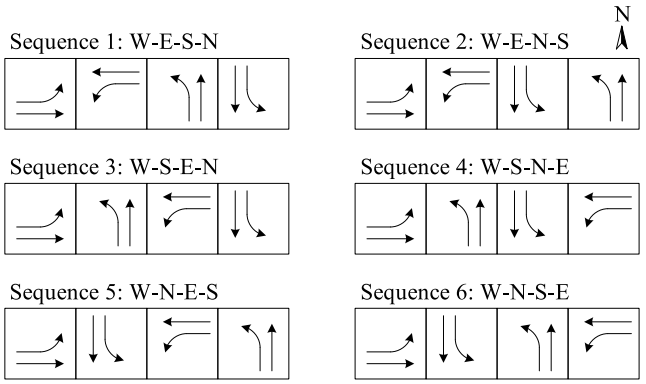

FIGURE 2. Six possible kinds of phase sequences in split phasing.

phasing is used. In Fig. 2, the term "W-E-S-N" represents one kind of phase sequence and means traffic movements in the west, east, south, and north approaches receive the right-of-way in turn. Other terms can be explained similarly. Obviously, phase sequences in the W-E and S-N directions of an intersection are interrelated when the split phasing is in use.

3) *Mixed Phasing:* The concept of a mixed phasing scheme means that some intersections in the traffic network operate with the NEMA phasing and some operate with the split phasing.

B. TYPES OF TRAFFIC NETWORKS

Depending on whether there are closed loops, traffic networks are categorized into closed traffic networks, unclosed traffic networks, and mixed traffic networks, as illustrated in Fig. 3(a), (b) and (c), respectively. In Fig. 3, directions from west to east or from south to north along an arterial are referred to as outbound. In the opposite directions,

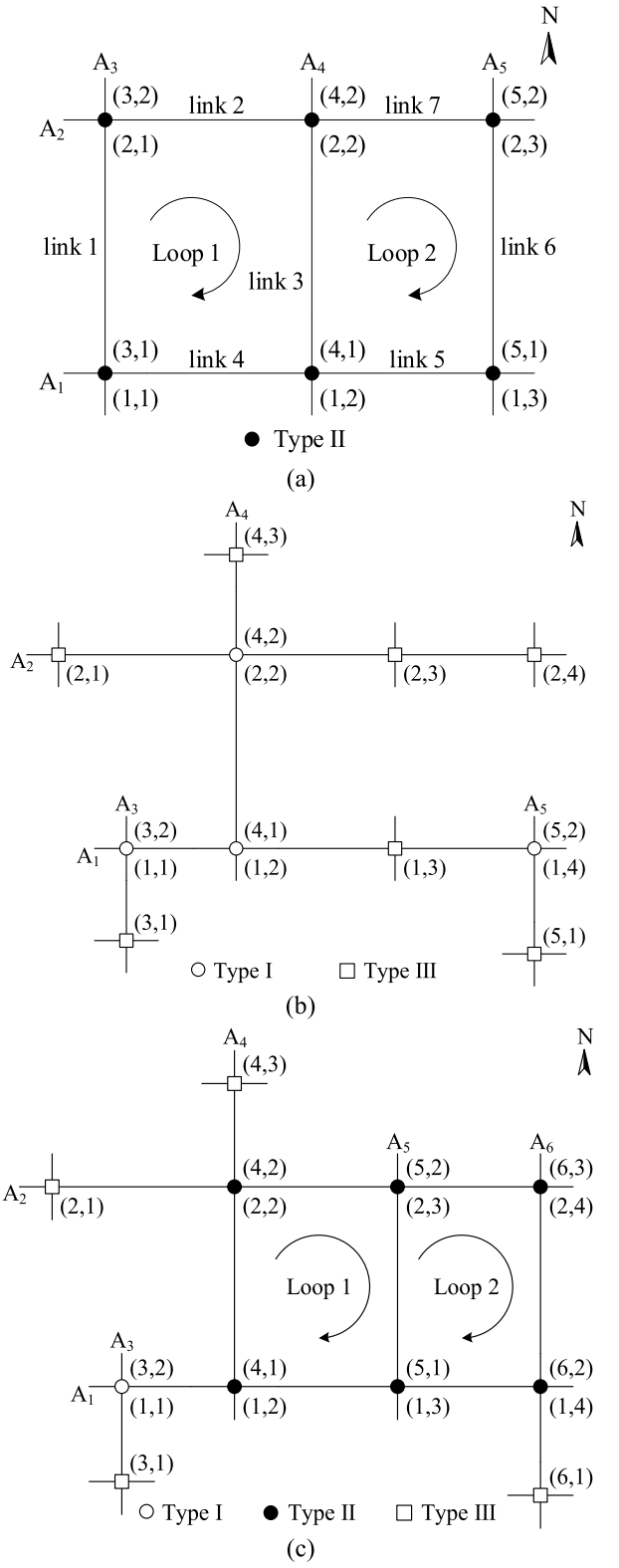

FIGURE 3. Examples of different types of traffic networks. (a) Example of a closed traffic network. (b) Example of an unclosed traffic network. (c) Example of a mixed traffic network.

they are referred to as inbound. The notation (i, j) represents the jth intersection on the ith arterial A_i, and j increases sequentially from the value of 1 in the outbound. According to this numbering convention, some intersections may have two different notations, but they denote the same intersection.

1) *Closed Traffic Network:* A closed traffic network is defined as a network in which each intersection is located in one or more closed loops consisting of more than two links. In Fig. 3(a), there are two closed loops: loops 1 and 2. Loop 1 consists of four links: links 1, 2, 3 and 4; loop 2 also consists of four links: links 3, 5, 6 and 7. It is clear that each intersection shown in Fig. 3(a) is located in loops 1 or 2. In particular, intersections on A_4 are located in both loops 1 and 2.

2) *Unclosed Traffic Network:* An unclosed traffic network is defined as a network in which there are no closed loops. It is easy to see that there are no closed loops in the traffic network illustrated in Fig. 3(b). That is to say, all the intersections in Fig. 3(b) are not located in one or more closed loops.

3) *Mixed Traffic Network:* A mixed traffic network is a hybrid of closed and unclosed traffic networks. That is, some intersections are located in one or more closed loops, and some are not. For example, as illustrated in Fig. 3(c), (1, 2), (1, 3), (1, 4), (2, 2), (2, 3), and (2, 4) are located in closed loops 1 or 2 and the rest of intersections are not.

C. INTERSECTION CLASSIFICATION

Based on their locations in the traffic network, intersections can be divided into three different types: Types I, II, and III. Type I: intersections that are located in two arterials along which bandwidth optimization will be conducted, and they are not located in closed loops. Type II: intersections that are located in two arterials along which bandwidth optimization will be conducted, and they are located in one or more closed loops. Type III: intersections that are only located in one arterial along which bandwidth optimization will be conducted. In Fig. 3, the empty circles, the solid circles, and the empty squares represent intersections that belong to Types I, II, and III, respectively. The main reason for classifying intersections is to conveniently describe the phase sequence constraints (see Section IV).

III. PROBLEM DESCRIPTION

The split phasing is a commonly used phasing scheme for signalized intersections. The advantages of split phasing have been elaborated in Section I. However, existing network bandwidth-based models mostly optimize signal coordination variables under NEMA phasing and rarely study the network bandwidth optimization problems systematically under the split phasing. In addition, the existing network bandwidth-based models mainly focus on the closed traffic networks but there are not only closed traffic networks but also unclosed or mixed traffic networks in the real world. To address these problems, this paper presents six different network bandwidth optimization models, called Models 1–6. In details,

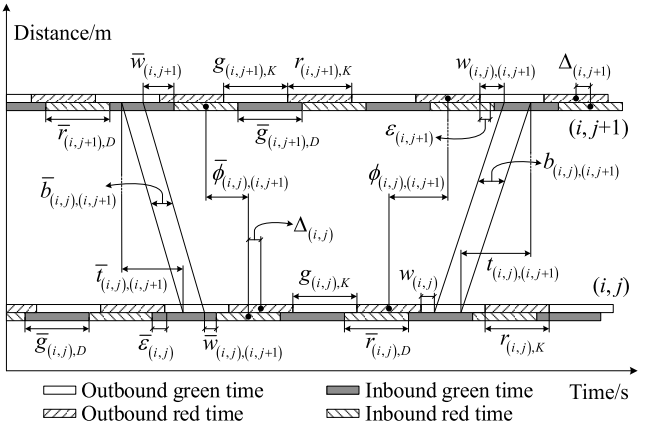

FIGURE 4. Time–space diagram for the proposed models.

Models 1 and 2 can be applied for bandwidth maximization problems under the split and mixed phasing scheme in closed traffic networks. The same problems in unclosed and mixed traffic networks can be solved by applying Models 3 and 4 and Models 5 and 6, respectively.

IV. MODEL FORMULATION

The proposed models are built on traffic networks where the numbering rules of the intersections are the same as those shown in Fig. 3. Fig. 4 shows the spatial-temporal relationships among the signal coordination control parameters and variables of adjacent intersections. Symbols involved in Fig. 4 are listed in Table 1.

In TABLE 1, $g_{(i,j),K}$, $\overline{g}_{(i,j),D}$, $r_{(i,j),K}$, $\overline{r}_{(i,j),D}$, $t_{(i,j),(i,j+1)}$, $\underline{t}_{(i,j),(i,j+1)}$, $\varepsilon_{(i,j)}$ and $\overline{\varepsilon}_{(i,j)}$ are input parameters; $b_{(i,j),(i,j+1)}$, $\overline{b}_{(i,j),(i,j+1)}$, $w_{(i,j)}$, $w_{(i,j),(i,j+1)}$, $\overline{w}_{(i,j),(i,j+1)}$, and $\overline{w}_{(i,j+1)}$ are decision variables. $\phi_{(i,j),(i,j+1)}$, $\overline{\phi}_{(i,j),(i,j+1)}$ and $\Delta_{(i,j)}$ are derived variables. $\phi_{(i,j),(i,j+1)}$ can be expressed by input parameters, $r_{(i,j),K}$, $r_{(i,j+1),K}$ and $t_{(i,j),(i,j+1)}$, and decision variables, $w_{(i,j)}$ and $w_{(i,j),(i,j+1)}$. $\overline{\phi}_{(i,j),(i,j+1)}$ can also be expressed by input parameters, $\overline{r}_{(i,j),D}$, $\overline{r}_{(i,j+1),D}$ and $\overline{t}_{(i,j),(i,j+1)}$, and decision variables, $\overline{w}_{(i,j),(i,j+1)}$ and $\overline{w}_{(i,j+1)}$. $\Delta_{(i,j)}$ are intranode offset variable and can be expressed by 0/1 variables, red and green times. Different values of the 0/1 variables can result in different phase sequences.

A. OBJECTIVE FUNCTION

As discussed previously, the objective function of the developed models can be formulated as

$$\max B = \sum_{i=1}^{M} \sum_{j=1}^{N_i-1} \left(\alpha_{(i,j),(i,j+1)} b_{(i,j),(i,j+1)} + \overline{\alpha}_{(i,j),(i,j+1)} \overline{b}_{(i,j),(i,j+1)} \right), \quad (1)$$

where M is the number of arterials in the traffic networks, N_i is the number of intersections on the ith arterial, $\alpha_{(i,j),(i,j+1)}$ is the weighting factor for the outbound bandwidth, and $\overline{\alpha}_{(i,j),(i,j+1)}$ is the weighting factor for the inbound

TABLE 1. Definitions of key symbols.

Symbols	Definition
$g_{(i,j),K}\left[\overline{g}_{(i,j),D}\right]$	Outbound [inbound] green time for movement K [D] at (i, j). K={WT, WL, ST, SL} and D={ET, EL, NT, NL}. WT [ST] and WL [SL] denote the through and left-turn movements respectively in the west [south] approach. ET [NT] and EL [NL] denote the through and left-turn movements in the east [north] approach. $g_{(i,j),K}=g^{\text{NEMA}}_{(i,j),K}\left[g^{\text{Split}}_{(i,j),K}\right]$ when (i, j) operates with NEMA [split] phasing. $\overline{g}_{(i,j),D}=\overline{g}^{\text{NEMA}}_{(i,j),D}\left[\overline{g}^{\text{Split}}_{(i,j),D}\right]$ when (i, j) operates with NEMA [split] phasing (cycles).
$r_{(i,j),K}\left[\overline{r}_{(i,j),D}\right]$	Outbound [inbound] red time for movement K [D] at (i, j). $r_{(i,j),K}=r^{\text{NEMA}}_{(i,j),K}\left[r^{\text{Split}}_{(i,j),K}\right]$ when (i, j) operates with NEMA [split] phasing. $\overline{r}_{(i,j),D}=\overline{r}^{\text{NEMA}}_{(i,j),D}\left[\overline{r}^{\text{Split}}_{(i,j),D}\right]$ when (i, j) operates with NEMA [split] phasing(cycles).
$t_{(i,j),(i,j+1)}\left[\overline{t}_{(i,j),(i,j+1)}\right]$	Outbound [inbound] travel time between (i, j) and $(i, j+1)$ (cycles).
$\varepsilon_{(i,j)}\left[\overline{\varepsilon}_{(i,j)}\right]$	Outbound [inbound] initial queue clearance time at (i, j) (cycles).
$b_{(i,j),(i,j+1)}\left[\overline{b}_{(i,j),(i,j+1)}\right]$	Outbound [inbound] bandwidth between (i, j) and $(i, j+1)$ (cycles).
$w_{(i,j)}\left[w_{(i,j),(i,j+1)}\right]$	Time from the right side of outbound red time at (i, j)[$(i, j+1)$] to the left side of the outbound bandwidth (cycles).
$\overline{w}_{(i,j),(i,j+1)}\left[\overline{w}_{(i,j+1)}\right]$	Time from the left side of inbound red time at (i, j)[$(i, j+1)$] to the right side of the inbound bandwidth (cycles).
$\phi_{(i,j),(i,j+1)}\left[\overline{\phi}_{(i,j),(i,j+1)}\right]$	Time from the center of an outbound [inbound] red time at (i, j) to the center of the nearest outbound [inbound] red time at $(i, j+1)$ (cycles).
$\Delta_{(i,j)}$	Time difference between the center of the outbound red time and the nearest center of the inbound red time at (i, j). It is positive if the center of the outbound red time locates in the right of the center of the inbound red time. Otherwise, it is negative (cycles).

bandwidths. The weighting factors can be calculated as follows:

$$\left.\begin{aligned}\alpha_{(i,j),(i,j+1)}&=\frac{V_{(i,j+1)}}{S_{(i,j+1)}}\\ \overline{\alpha}_{(i,j),(i,j+1)}&=\frac{\overline{V}_{(i,j)}}{\overline{S}_{(i,j)}}\end{aligned}\right\}, \tag{2}$$

where $V_{(i,j+1)}$ [$\overline{V}_{(i,j)}$] represents outbound [inbound] through traffic volumes at $(i, j+1)$ [(i, j)], and $S_{(i,j+1)}$ [$\overline{S}_{(i,j)}$] represents outbound [inbound] through saturation flow rates at $(i, j+1)$ [(i, j)]. Additionally, the values of $\alpha_{(i,j),(i,j+1)}$ and $\overline{\alpha}_{(i,j),(i,j+1)}$ can also be set by traffic engineers based on the practical control needs.

B. MODEL CONSTRAINTS

1) *Bandwidth Ratio Constraints:* To avoid the occurrence of a very small or a near-zero link bandwidth of one direction, the following constraint should be satisfied:

$$\begin{aligned}\left(1-k_{(i,j),(i,j+1)}\right)\overline{b}_{(i,j),(i,j+1)}\geq\left(1-k_{(i,j),(i,j+1)}\right)k_{(i,j),(i,j+1)}b_{(i,j),(i,j+1)},\\ i=1,\ldots,M;j=1,\ldots,N_i-1,\end{aligned} \tag{3}$$

where

$$k_{(i,j),(i,j+1)}=\frac{\overline{V}_{(i,j)}}{V_{(i,j+1)}}. \tag{4}$$

It should be noted that equation (3) must be replaced by $b_{(i,j),(i,j+1)}=\overline{b}_{(i,j),(i,j+1)}$ when $k_{(i,j),(i,j+1)}=1$. Similarly, the values of $k_{(i,j),(i,j+1)}$ can also be specified by traffic engineers based on the practical control needs.

2) *Interference Constraints:* To ensure that the left and right boundaries of a progression band are located within the green time and do not interfere with the red time, the corresponding constraints can be expressed as

$$\left.\begin{aligned}w_{(i,j)}+b_{(i,j),(i,j+1)}&\leq g_{(i,j),K}\\ \overline{w}_{(i,j),(i,j+1)}+\overline{b}_{(i,j),(i,j+1)}&\leq\overline{g}_{(i,j),D}-\overline{\varepsilon}_{(i,j)}\\ w_{(i,j),(i,j+1)}+b_{(i,j),(i,j+1)}&\leq g_{(i,j+1),K}\\ \overline{w}_{(i,j+1)}+\overline{b}_{(i,j),(i,j+1)}&\leq\overline{g}_{(i,j+1),D}\end{aligned}\right\},\quad i=1,\ldots,M;j=1,\ldots,N_i-1. \tag{5}$$

3) *Nonnegative Constraints:* Based on the definitions of variables $w_{(i,j)}$, $\overline{w}_{(i,j),(i,j+1)}$, $w_{(i,j),(i,j+1)}$, $\overline{w}_{(i,j+1)}$, $b_{(i,j),(i,j+1)}$, $\overline{b}_{(i,j),(i,j+1)}$, $t_{(i,j),(i,j+1)}$ and $\overline{t}_{(i,j),(i,j+1)}$, they should satisfy the following constraints:

$$\left.\begin{aligned}&w_{(i,j)}\geq 0\\ &\overline{w}_{(i,j),(i,j+1)}\geq 0\\ &w_{(i,j),(i,j+1)}-\varepsilon_{(i,j+1)}\geq 0\\ &\overline{w}_{(i,j+1)}\geq 0\\ &b_{(i,j),(i,j+1)}\geq 0\\ &\overline{b}_{(i,j),(i,j+1)}\geq 0\\ &t_{(i,j),(i,j+1)}\geq 0\\ &\overline{t}_{(i,j),(i,j+1)}\geq 0\end{aligned}\right\},\ i=1,\ldots,M;j=1,\ldots,N_i-1. \tag{6}$$

4) *Arterial Loop Constraints:* The arterial loop constraints arise because all intersections are operated with a common cycle time. As shown in Fig. 4, the center of the inbound red time at (i, j), the center of the outbound red time at (i, j), the center of the inbound red time at $(i, j+1)$ and the center of the outbound red time at $(i, j+1)$ can form an arterial loop, which can be mathematically expressed by

$$\overline{\phi}_{(i,j),(i,j+1)}+\Delta_{(i,j)}+\phi_{(i,j),(i,j+1)}-\Delta_{(i,j+1)}=m_{(i,j),(i,j+1)}, \tag{7}$$

where $m_{(i,j),(i,j+1)}$ is an integer variable that represents an integer multiple of the common cycle length.

As shown in Fig. 4, variables $\phi_{(i,j),(i,j+1)}$ and $\overline{\phi}_{(i,j),(i,j+1)}$ can be formulated by

$$\begin{aligned}\phi_{(i,j),(i,j+1)}&=0.5r_{(i,j),K}+w_{(i,j)}+t_{(i,j),(i,j+1)}\\ &\quad-w_{(i,j),(i,j+1)}-0.5r_{(i,j+1),K},\end{aligned} \tag{8}$$

$$\begin{aligned}\overline{\phi}_{(i,j),(i,j+1)}&=0.5\overline{r}_{(i,j),D}+\overline{w}_{(i,j),(i,j+1)}+\overline{t}_{(i,j),(i,j+1)}\\ &\quad-\overline{w}_{(i,j+1)}-0.5\overline{r}_{(i,j+1),D}.\end{aligned} \tag{9}$$

By substituting (8) and (9) into (7) to eliminate the internode offsets $\phi_{(i,j),(i,j+1)}$ and $\overline{\phi}_{(i,j),(i,j+1)}$, the arterial loop constraints can be updated to the following equation:

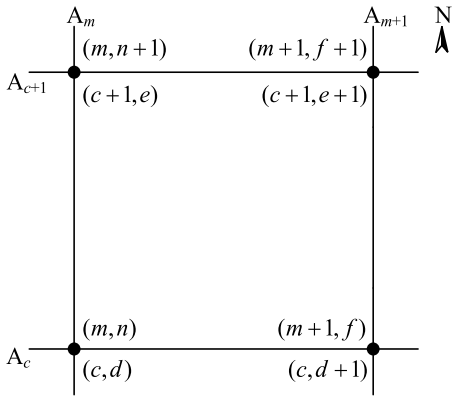

FIGURE 5. Network closed loops of four intersecting segments.

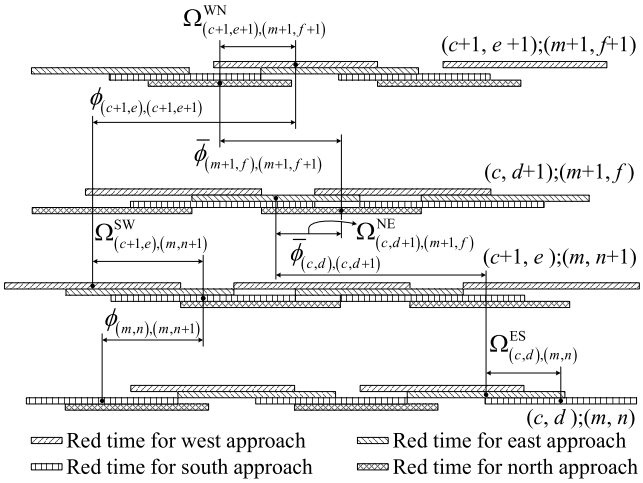

FIGURE 6. Geometry of network clockwise loop constraint.

$$
\begin{aligned}
&0.5\left(r_{(i,j),K}+\bar{r}_{(i,j),D}\right)-0.5\left(r_{(i,j+1),K}+\bar{r}_{(i,j+1),D}\right)\\
&\quad+\left(w_{(i,j)}+\overline{w}_{(i,j),(i,j+1)}\right)-\left(w_{(i,j),(i,j+1)}+\overline{w}_{(i,j+1)}\right)\\
&\quad+\left(t_{(i,j),(i,j+1)}+\bar{t}_{(i,j),(i,j+1)}\right)+\Delta_{(i,j)}-\Delta_{(i,j+1)}=m_{(i,j),(i,j+1)},\\
&\quad i=1,\ldots,M;j=1,\ldots,N_i-1, \qquad (10)
\end{aligned}
$$

where $\Delta_{(i,j)}=\Delta^{\mathrm{NEMA}}_{(i,j)}$ [$\Delta_{(i,j)}=\Delta^{\mathrm{Split}}_{(i,j)}$] when (i, j) operates with the NEMA [split] phasing. The formulas for $\Delta^{\mathrm{NEMA}}_{(i,j)}$ and $\Delta^{\mathrm{Split}}_{(i,j)}$ are given in the *"6) Phase Sequence Constraints"* subsection.

5) *Network Loop Constraints:* The principle of arterial loop constraints also applies to network loop constraints. As shown in Fig. 5, the four intersecting segments form two closed loops, namely clockwise and anticlockwise loops. The clockwise loop constraint is equivalent to the anticlockwise one. Therefore, only the clockwise loop constraint is needed to be described. According to Fig. 6, the clockwise loop constraint can be expressed as

$$
\begin{aligned}
&\phi_{(m,n),(m,n+1)}-\Omega^{\mathrm{SW}}_{(c+1,e),(m,n+1)}+\phi_{(c+1,e),(c+1,e+1)}\\
&\quad-\Omega^{\mathrm{WN}}_{(c+1,e+1),(m+1,f+1)}+\overline{\phi}_{(m+1,f),(m+1,f+1)}\\
&\quad-\Omega^{\mathrm{NE}}_{(c,d+1),(m+1,f)}+\overline{\phi}_{(c,d),(c,d+1)}-\Omega^{\mathrm{ES}}_{(c,d),(m,n)}\\
&\quad=n_{(c,d),(c+1,e+1)}, \qquad (11)
\end{aligned}
$$

where $n_{(c,d),(c+1,e+1)}$ is an integer variable, and $\Omega^{F_1F_2}$ (for simplicity the subscript is dropped) is defined as the time difference between the center of the red time for F_1 (F_1={S, W, N, E}) at an intersection and the nearest center of the red time for F_2 (F_2 ={W, N, E, S}) at the same intersection. It is positive if the center of the red time for F_1 is to the right of the center of the red time for F_2. Otherwise, it is negative. Symbols S, W, N, and E in F_1 and F_2 represent the through movement at the south, west, north, and east approaches, respectively. In addition, note that there is a sequential one-to-one match between the elements in F_1 and those in F_2.

Similarly, the internode offset variables in (11) can also be eliminated, and the network loop constraints can further be updated to

$$
\begin{aligned}
&0.5\left(r_{(m,n),\mathrm{ST}}+r_{(c+1,e),\mathrm{WT}}+\bar{r}_{(m+1,f),\mathrm{NT}}+\bar{r}_{(c,d),\mathrm{ET}}\right)\\
&\quad-0.5\left(r_{(m,n+1),\mathrm{ST}}+r_{(c+1,e+1),\mathrm{WT}}+\bar{r}_{(m+1,f+1),\mathrm{NT}}+\bar{r}_{(c,d+1),\mathrm{ET}}\right)\\
&\quad+\left(w_{(m,n)}+w_{(c+1,e)}+\overline{w}_{(m+1,f),(m+1,f+1)}+\overline{w}_{(c,d),(c,d+1)}\right)\\
&\quad-\left(w_{(m,n),(m,n+1)}+w_{(c+1,e),(c+1,e+1)}+\overline{w}_{(m+1,f+1)}+\overline{w}_{(c,d+1)}\right)\\
&\quad+\left(t_{(m,n),(m,n+1)}+t_{(c+1,e),(c+1,e+1)}+\bar{t}_{(m+1,f),(m+1,f+1)}\right.\\
&\quad\left.+\bar{t}_{(c,d),(c,d+1)}\right)-\Omega^{\mathrm{SW}}_{(c+1,e),(m,n+1)}-\Omega^{\mathrm{WN}}_{(c+1,e+1),(m+1,f+1)}\\
&\quad-\Omega^{\mathrm{NE}}_{(c,d+1),(m+1,f)}-\Omega^{\mathrm{ES}}_{(c,d),(m,n)}\\
&\quad=n_{(c,d),(c+1,e+1)},\ c\in\{1,\ldots,M\},\ m\in\{1,\ldots,M\},\ d\in\{1,\ldots,N_c\},\\
&\quad n\in\{1,\ldots,N_m\},\ e\in\{1,\ldots,N_{c+1}\},f\in\{1,\ldots,N_{m+1}\}. \qquad (12)
\end{aligned}
$$

Similarly, $\Omega^{F_1F_2}=\Omega^{\mathrm{NEMA},F_1F_2}$ [$\Omega^{F_1F_2}=\Omega^{\mathrm{Split},F_1F_2}$] when an intersection operates with the NEMA [split] phasing. The general formulas of $\Omega^{\mathrm{NEMA},F_1F_2}$ and $\Omega^{\mathrm{Split},F_1F_2}$ are also given in the "6) *Phase Sequence Constraints"* subsection.

6) *Phase Sequence Constraints:* Phase sequences can be optimized by giving general formulas for the variables Δ and Ω(for simplicity, the superscripts and subscripts are dropped) due to their close relation to the phase sequences. The general formulas can be developed by introducing 0/1 variables. It is noticeable that the intersections of different types have different numbers of Δ and Ω. For the convenience of describing the phase sequence constraints, suppose that subscripts (p, q) and (r, s) of Δ in this subsection represent the intersection located in the W-E and S-N arterials, respectively.

A) General Formulas for $\Delta^{NEMA}_{(p,q)}$ and $\Delta^{NEMA}_{(r,s)}$ for Intersection of Type I: In the light of the MAXBAND [4] or MULTIBAND [5] model, the general formulas for $\Delta^{\mathrm{NEMA}}_{(p,q)}$ and $\Delta^{\mathrm{NEMA}}_{(r,s)}$ for an intersection of Type I are expressed by

$$
\begin{aligned}
\Delta^{\mathrm{NEMA}}_{(p,q)}&=y_{(p,q)}g^{\mathrm{NEMA}}_{(p,q),\mathrm{WL}}-0.5g^{\mathrm{NEMA}}_{(p,q),\mathrm{WL}}\\
&\quad-z_{(p,q)}\bar{g}^{\mathrm{NEMA}}_{(p,q),\mathrm{EL}}+0.5\bar{g}^{\mathrm{NEMA}}_{(p,q),\mathrm{EL}}, \qquad (13)\\
\Delta^{\mathrm{NEMA}}_{(r,s)}&=y_{(r,s)}g^{\mathrm{NEMA}}_{(r,s),\mathrm{SL}}-0.5g^{\mathrm{NEMA}}_{(r,s),\mathrm{SL}}\\
&\quad-z_{(r,s)}\bar{g}^{\mathrm{NEMA}}_{(r,s),\mathrm{NL}}+0.5\bar{g}^{\mathrm{NEMA}}_{(r,s),\mathrm{NL}}, \qquad (14)
\end{aligned}
$$

where $y_{(p,q)}$, $z_{(p,q)}$, $y_{(r,s)}$, and $z_{(r,s)}$ are 0/1 variables through which the phase sequence can be optimized, which can be seen in Table 2.

TABLE 2. Relationships between 0/1 variables and phase sequences in NEMA phasing for an intersection of type I.

Phase sequence	$y_{(p,q)}$	$z_{(p,q)}$	$y_{(r,s)}$	$z_{(r,s)}$
1	0	1	0	1
2	1	0	1	0
3	0	0	0	0
4	1	1	1	1

TABLE 3. Formulas for $\Delta^{\text{Split}}_{(p,q)}$ and $\Delta^{\text{Split}}_{(r,s)}$ under each phase sequence in split phasing.

Phase sequence	$\Delta^{\text{Split}}_{(p,q)}$	$\Delta^{\text{Split}}_{(r,s)}$
1	$-0.5\left(g^{\text{Split}}_{(p,q),\text{WT}}+\overline{g}^{\text{Split}}_{(p,q),\text{ET}}\right)$	$-0.5\left(g^{\text{Split}}_{(r,s),\text{ST}}+\overline{g}^{\text{Split}}_{(r,s),\text{NT}}\right)$
2	$-0.5\left(g^{\text{Split}}_{(p,q),\text{WT}}+\overline{g}^{\text{Split}}_{(p,q),\text{ET}}\right)$	$0.5\left(g^{\text{Split}}_{(r,s),\text{ST}}+\overline{g}^{\text{Split}}_{(r,s),\text{NT}}\right)$
3	$\begin{cases}0.5\left(g^{\text{Split}}_{(p,q),\text{WT}}+\overline{g}^{\text{Split}}_{(p,q),\text{ET}}\right)\\ +\overline{g}^{\text{Split}}_{(r,s),\text{NT}}, g^{\text{Split}}_{(r,s),\text{ST}}\geq\overline{g}^{\text{Split}}_{(r,s),\text{NT}}\\ -0.5\left(g^{\text{Split}}_{(p,q),\text{WT}}+\overline{g}^{\text{Split}}_{(p,q),\text{ET}}\right)\\ -g^{\text{Split}}_{(r,s),\text{ST}}, g^{\text{Split}}_{(r,s),\text{ST}}<\overline{g}^{\text{Split}}_{(r,s),\text{NT}}\end{cases}$	$\begin{cases}0.5\left(g^{\text{Split}}_{(r,s),\text{ST}}+\overline{g}^{\text{Split}}_{(r,s),\text{NT}}\right)\\ +g^{\text{Split}}_{(p,q),\text{WT}}, \overline{g}^{\text{Split}}_{(p,q),\text{ET}}\geq g^{\text{Split}}_{(p,q),\text{WT}}\\ -0.5\left(g^{\text{Split}}_{(r,s),\text{ST}}+\overline{g}^{\text{Split}}_{(r,s),\text{NT}}\right)\\ -\overline{g}^{\text{Split}}_{(p,q),\text{ET}}, \overline{g}^{\text{Split}}_{(p,q),\text{ET}}<g^{\text{Split}}_{(p,q),\text{WT}}\end{cases}$
4	$0.5\left(g^{\text{Split}}_{(p,q),\text{WT}}+\overline{g}^{\text{Split}}_{(p,q),\text{ET}}\right)$	$-0.5\left(g^{\text{Split}}_{(r,s),\text{ST}}+\overline{g}^{\text{Split}}_{(r,s),\text{NT}}\right)$
5	$\begin{cases}-0.5\left(g^{\text{Split}}_{(p,q),\text{WT}}+\overline{g}^{\text{Split}}_{(p,q),\text{ET}}\right)-\\ \overline{g}^{\text{Split}}_{(r,s),\text{NT}}, g^{\text{Split}}_{(r,s),\text{ST}}\geq\overline{g}^{\text{Split}}_{(r,s),\text{NT}}\\ 0.5\left(g^{\text{Split}}_{(p,q),\text{WT}}+\overline{g}^{\text{Split}}_{(p,q),\text{ET}}\right)+\\ g^{\text{Split}}_{(r,s),\text{ST}}, g^{\text{Split}}_{(r,s),\text{ST}}<\overline{g}^{\text{Split}}_{(r,s),\text{NT}}\end{cases}$	$\begin{cases}-0.5\left(g^{\text{Split}}_{(r,s),\text{ST}}+\overline{g}^{\text{Split}}_{(r,s),\text{NT}}\right)\\ -g^{\text{Split}}_{(p,q),\text{WT}}, \overline{g}^{\text{Split}}_{(p,q),\text{ET}}\geq g^{\text{Split}}_{(p,q),\text{WT}}\\ 0.5\left(g^{\text{Split}}_{(r,s),\text{ST}}+\overline{g}^{\text{Split}}_{(r,s),\text{NT}}\right)\\ +\overline{g}^{\text{Split}}_{(p,q),\text{ET}}, \overline{g}^{\text{Split}}_{(p,q),\text{ET}}<g^{\text{Split}}_{(p,q),\text{WT}}\end{cases}$
6	$0.5\left(g^{\text{Split}}_{(p,q),\text{WT}}+\overline{g}^{\text{Split}}_{(p,q),\text{ET}}\right)$	$0.5\left(g^{\text{Split}}_{(r,s),\text{ST}}+\overline{g}^{\text{Split}}_{(r,s),\text{NT}}\right)$

It should be noted that the determination of the optimal phase sequences in the W-E and S-N directions is independent of each other at an intersection of Type I when the NEMA phasing is used.

B) General Formulas for $\Delta^{Split}_{(p,q)}$ and $\Delta^{Split}_{(r,s)}$ for Intersection of Type I: Based on similar logic to that when deriving formulas for $\Delta^{\text{NEMA}}_{(p,q)}$ or $\Delta^{\text{NEMA}}_{(r,s)}$, formulas for $\Delta^{\text{Split}}_{(p,q)}$ and $\Delta^{\text{Split}}_{(r,s)}$ under each phase sequence illustrated in Fig. 2 are directly shown in Table 3 and their general formulas can be formulated as

$$\Delta^{\text{Split}}_{(p,q)}=\begin{cases}\sum_{h=1}^{3}\left(v_{(p,q),h}-0.5u_{(p,q),h}\right)\left(g^{\text{Split}}_{(p,q),\text{WT}}+\overline{g}^{\text{Split}}_{(p,q),\text{ET}}\right)\\ +\left(2v_{(p,q),3}-u_{(p,q),3}\right)\overline{g}^{\text{Split}}_{(r,s),\text{NT}}, g^{\text{Split}}_{(r,s),\text{ST}}\geq\overline{g}^{\text{Split}}_{(r,s),\text{NT}}\\ \left[\begin{array}{l}\sum_{h=1}^{2}\left(v_{(p,q),h}-0.5u_{(p,q),h}\right)\\ +\left(0.5u_{(p,q),3}-v_{(p,q),3}\right)\end{array}\right]\left(g^{\text{Split}}_{(p,q),\text{WT}}+\overline{g}^{\text{Split}}_{(p,q),\text{ET}}\right)\\ +\left(u_{(p,q),3}-2v_{(p,q),3}\right)g^{\text{Split}}_{(r,s),\text{ST}}, g^{\text{Split}}_{(r,s),\text{ST}}<\overline{g}^{\text{Split}}_{(r,s),\text{NT}}\end{cases}, \tag{15}$$

TABLE 4. Relationships between 0/1 variables and phase sequences in split phasing for an intersection of type I.

Phase sequence	$u_{(p,q),1}$ $u_{(r,s),1}$	$u_{(p,q),2}$ $u_{(r,s),2}$	$u_{(p,q),3}$ $u_{(r,s),3}$	$v_{(p,q),1}$ $v_{(r,s),1}$	$v_{(p,q),2}$ $v_{(r,s),2}$	$v_{(p,q),3}$ $v_{(r,s),3}$
1	1	0	0	0	/	/
2	0	1	0	/	0	/
3	0	0	1	/	/	1
4	0	1	0	/	1	/
5	0	0	1	/	/	0
6	1	0	0	1	/	/

$$\Delta^{\text{Split}}_{(r,s)}=\begin{cases}\sum_{h=1}^{3}(-1)^{h+1}\left(v_{(r,s),h}-0.5u_{(r,s),h}\right)\left(g^{\text{Split}}_{(r,s),\text{ST}}+\overline{g}^{\text{Split}}_{(r,s),\text{NT}}\right)\\ +\left(2v_{(r,s),3}-u_{(r,s),3}\right)g^{\text{Split}}_{(p,q),\text{WT}}, \overline{g}^{\text{Split}}_{(p,q),\text{ET}}\geq g^{\text{Split}}_{(p,q),\text{WT}}\\ \left[\begin{array}{l}\left(v_{(r,s),1}-0.5u_{(r,s),1}\right)\\ +\sum_{h=2}^{3}\left(0.5u_{(r,s),h}-v_{(r,s),h}\right)\end{array}\right]\left(g^{\text{Split}}_{(r,s),\text{ST}}+\overline{g}^{\text{Split}}_{(r,s),\text{NT}}\right)\\ +\left(u_{(r,s),3}-2v_{(r,s),3}\right)\overline{g}^{\text{Split}}_{(p,q),\text{ET}}, \overline{g}^{\text{Split}}_{(p,q),\text{ET}}<g^{\text{Split}}_{(p,q),\text{WT}}\end{cases}. \tag{16}$$

Furthermore, 0/1 variables in (15) and (16) should satisfy the following constraints to exclude the ineligible 0/1 combinations:

$$\left.\begin{array}{l}\sum_{h=1}^{3}u_{(p,q),h}=1\\ \sum_{h=1}^{3}u_{(r,s),h}=1\\ u_{(p,q),h}-v_{(p,q),h}\geq 0, \forall h\leq 3\\ u_{(r,s),h}-v_{(r,s),h}\geq 0, \forall h\leq 3\end{array}\right\}. \tag{17}$$

It is easy to see that phase sequences in the W-E and S-N directions are not independent at an intersection of Type I when the split phasing is used. That is, there should be a mutual phase sequence constraint to ensure that the optimal phase sequence obtained in the W-E direction is the same as that obtained in the S-N direction. The mutual phase sequence constraint can be described by

$$\left.\begin{array}{l}u_{(p,q),h}=u_{(r,s),h}, \forall h\leq 3\\ v_{(p,q),h}=v_{(r,s),h}, \forall h\leq 3\end{array}\right\}. \tag{18}$$

Table 4 shows how the introduced 0/1 variables select the optimal phase sequence in the split phasing for an intersection of Type I.

C) General Formulas for $\Delta^{NEMA}_{(p,q)}$, $\Delta^{NEMA}_{(r,s)}$ and Ω for Intersection of Type II: It is easy to see that under the NEMA phasing, the phase sequences in the W-E and S-N directions are interdependent with each other at an intersection of Type II. In other words, the optimal phase sequences are simultaneously determined by $\Delta^{\text{NEMA}}_{(p,q)}$, $\Delta^{\text{NEMA}}_{(r,s)}$, and Ω.

The general formulas for $\Delta^{\text{NEMA}}_{(p,q)}$ and $\Delta^{\text{NEMA}}_{(r,s)}$ for an intersection of Type II can be expressed by

$$\Delta_{(p,q)}^{\text{NEMA}} = \sum_{h=1}^{4}\left(y_{(r,s),h}^{(p,q)} - 0.5z_{(r,s),h}^{(p,q)}\right)\left(g_{(p,q),\text{WL}}^{\text{NEMA}} + \bar{g}_{(p,q),\text{EL}}^{\text{NEMA}}\right) + \sum_{h=5}^{8}\left(y_{(r,s),h}^{(p,q)} - 0.5z_{(r,s),h}^{(p,q)}\right)\left(g_{(p,q),\text{WL}}^{\text{NEMA}} - \bar{g}_{(p,q),\text{EL}}^{\text{NEMA}}\right), \quad (19)$$

$$\Delta_{(r,s)}^{\text{NEMA}} = \left[\begin{array}{l}\sum_{h}^{1,5}\left(y_{(r,s),h}^{(p,q)} - 0.5z_{(r,s),h}^{(p,q)}\right)+ \\ \sum_{h}^{2,6}\left(0.5z_{(r,s),h}^{(p,q)} - y_{(r,s),h}^{(p,q)}\right)\end{array}\right]\left(g_{(r,s),\text{SL}}^{\text{NEMA}} + \bar{g}_{(r,s),\text{NL}}^{\text{NEMA}}\right) + \left[\begin{array}{l}\sum_{h}^{3,7}\left(y_{(r,s),h}^{(p,q)} - 0.5z_{(r,s),h}^{(p,q)}\right)+ \\ \sum_{h}^{4,8}\left(0.5z_{(r,s),h}^{(p,q)} - y_{(r,s),h}^{(p,q)}\right)\end{array}\right]\left(g_{(r,s),\text{SL}}^{\text{NEMA}} - \bar{g}_{(r,s),\text{NL}}^{\text{NEMA}}\right). \quad (20)$$

The general formulas for $\Omega_{(p,q),(r,s)}^{\text{NEMA,NE}}$, $\Omega_{(p,q),(r,s)}^{\text{NEMA,SW}}$, $\Omega_{(p,q),(r,s)}^{\text{NEMA,WN}}$, and $\Omega_{(p,q),(r,s)}^{\text{NEMA,ES}}$ for an intersection of Type II can be expressed, respectively, by

$$\Omega_{(p,q),(r,s)}^{\text{NEMA,NE}} = \begin{cases} \sum_{h}^{2,4,6,8}\left(z_{(r,s),h}^{(p,q)} - 2y_{(r,s),h}^{(p,q)}\right)\left(\begin{array}{l}0.5\bar{r}_{(r,s),\text{NT}}^{\text{NEMA}}- \\ 0.5\bar{r}_{(p,q),\text{ET}}^{\text{NEMA}} + \bar{g}_{(r,s),\text{NT}}^{\text{NEMA}}\end{array}\right) \\ \quad + \sum_{h}^{1,3,5,7}\left(z_{(r,s),h}^{(p,q)} - 2y_{(r,s),h}^{(p,q)}\right)\left(\begin{array}{l}0.5\bar{r}_{(r,s),\text{NT}}^{\text{NEMA}}+ \\ 0.5\bar{r}_{(p,q),\text{ET}}^{\text{NEMA}} - g_{(p,q),\text{WL}}^{\text{NEMA}}\end{array}\right), \\ g_{(r,s),\text{SL}}^{\text{NEMA}} \le g_{(p,q),\text{WL}}^{\text{NEMA}} \\ \sum_{h}^{2,4,6,8}\left(z_{(r,s),h}^{(p,q)} - 2y_{(r,s),h}^{(p,q)}\right)\left(\begin{array}{l}0.5\bar{r}_{(r,s),\text{NT}}^{\text{NEMA}}- \\ 0.5\bar{r}_{(p,q),\text{ET}}^{\text{NEMA}} + \bar{g}_{(r,s),\text{NT}}^{\text{NEMA}}\end{array}\right) \\ \quad + \sum_{h}^{1,3,5,7}\left(2y_{(r,s),h}^{(p,q)} - z_{(r,s),h}^{(p,q)}\right)\left(\begin{array}{l}0.5\bar{r}_{(r,s),\text{NT}}^{\text{NEMA}}+ \\ 0.5\bar{r}_{(p,q),\text{ET}}^{\text{NEMA}} - g_{(r,s),\text{SL}}^{\text{NEMA}}\end{array}\right), \\ g_{(r,s),\text{SL}}^{\text{NEMA}} > g_{(p,q),\text{WL}}^{\text{NEMA}} \end{cases}, \quad (21)$$

$$\Omega_{(p,q),(r,s)}^{\text{NEMA,SW}} = \begin{cases} \left[\begin{array}{l}\sum_{h}^{2,3}\left(2y_{(r,s),h}^{(p,q)} - z_{(r,s),h}^{(p,q)}\right) \\ \quad + \sum_{h}^{5,8}\left(z_{(r,s),h}^{(p,q)} - 2y_{(r,s),h}^{(p,q)}\right)\end{array}\right]\left(\begin{array}{l}0.5r_{(r,s),\text{ST}}^{\text{NEMA}}- \\ 0.5r_{(p,q),\text{WT}}^{\text{NEMA}} + g_{(r,s),\text{ST}}^{\text{NEMA}}\end{array}\right) \\ \quad + \left[\begin{array}{l}\sum_{h}^{1,4}\left(2y_{(r,s),h}^{(p,q)} - z_{(r,s),h}^{(p,q)}\right) \\ \quad + \sum_{h}^{6,7}\left(z_{(r,s),h}^{(p,q)} - 2y_{(r,s),h}^{(p,q)}\right)\end{array}\right]\left(\begin{array}{l}0.5r_{(r,s),\text{ST}}^{\text{NEMA}}+ \\ 0.5r_{(p,q),\text{WT}}^{\text{NEMA}} - \bar{g}_{(p,q),\text{EL}}^{\text{NEMA}}\end{array}\right), \\ \bar{g}_{(r,s),\text{NL}}^{\text{NEMA}} \le \bar{g}_{(p,q),\text{EL}}^{\text{NEMA}} \\ \left[\begin{array}{l}\sum_{h}^{2,3}\left(2y_{(r,s),h}^{(p,q)} - z_{(r,s),h}^{(p,q)}\right) \\ \quad + \sum_{h}^{5,8}\left(z_{(r,s),h}^{(p,q)} - 2y_{(r,s),h}^{(p,q)}\right)\end{array}\right]\left(\begin{array}{l}0.5r_{(r,s),\text{ST}}^{\text{NEMA}}- \\ 0.5r_{(p,q),\text{WT}}^{\text{NEMA}} + g_{(r,s),\text{ST}}^{\text{NEMA}}\end{array}\right) \\ \quad + \left[\begin{array}{l}\sum_{h}^{1,4}\left(z_{(r,s),h}^{(p,q)} - 2y_{(r,s),h}^{(p,q)}\right) \\ \quad + \sum_{h}^{6,7}\left(2y_{(r,s),h}^{(p,q)} - z_{(r,s),h}^{(p,q)}\right)\end{array}\right]\left(\begin{array}{l}0.5r_{(r,s),\text{ST}}^{\text{NEMA}}+ \\ 0.5r_{(p,q),\text{WT}}^{\text{NEMA}} - \bar{g}_{(r,s),\text{NL}}^{\text{NEMA}}\end{array}\right), \\ \bar{g}_{(r,s),\text{NL}}^{\text{NEMA}} > \bar{g}_{(p,q),\text{EL}}^{\text{NEMA}} \end{cases}, \quad (22)$$

$$\Omega_{(p,q),(r,s)}^{\text{NEMA,WN}} = \begin{cases} \left[\begin{array}{l}\sum_{h}^{1,3}\left(z_{(r,s),h}^{(p,q)} - 2y_{(r,s),h}^{(p,q)}\right)+ \\ \sum_{h}^{6,8}\left(2y_{(r,s),h}^{(p,q)} - z_{(r,s),h}^{(p,q)}\right)\end{array}\right]\left(\begin{array}{l}0.5r_{(p,q),\text{WT}}^{\text{NEMA}}- \\ 0.5\bar{r}_{(r,s),\text{NT}}^{\text{NEMA}} + g_{(p,q),\text{WT}}^{\text{NEMA}}\end{array}\right) \\ \quad + \left[\begin{array}{l}\sum_{h}^{2,4}\left(z_{(r,s),h}^{(p,q)} - 2y_{(r,s),h}^{(p,q)}\right) \\ \quad + \sum_{h}^{5,7}\left(2y_{(r,s),h}^{(p,q)} - z_{(r,s),h}^{(p,q)}\right)\end{array}\right]\left(\begin{array}{l}0.5r_{(p,q),\text{WT}}^{\text{NEMA}}+ \\ 0.5\bar{r}_{(r,s),\text{NT}}^{\text{NEMA}} - \bar{g}_{(p,q),\text{EL}}^{\text{NEMA}}\end{array}\right), \\ g_{(r,s),\text{SL}}^{\text{NEMA}} \le \bar{g}_{(p,q),\text{EL}}^{\text{NEMA}} \\ \left[\begin{array}{l}\sum_{h}^{1,3}\left(z_{(r,s),h}^{(p,q)} - 2y_{(r,s),h}^{(p,q)}\right) \\ \quad + \sum_{h}^{6,8}\left(2y_{(r,s),h}^{(p,q)} - z_{(r,s),h}^{(p,q)}\right)\end{array}\right]\left(\begin{array}{l}0.5r_{(p,q),\text{WT}}^{\text{NEMA}}- \\ 0.5\bar{r}_{(r,s),\text{NT}}^{\text{NEMA}} + g_{(p,q),\text{WT}}^{\text{NEMA}}\end{array}\right) \\ \quad + \left[\begin{array}{l}\sum_{h}^{2,4}\left(2y_{(r,s),h}^{(p,q)} - z_{(r,s),h}^{(p,q)}\right) \\ \quad + \sum_{h}^{5,7}\left(z_{(r,s),h}^{(p,q)} - 2y_{(r,s),h}^{(p,q)}\right)\end{array}\right]\left(\begin{array}{l}0.5r_{(p,q),\text{WT}}^{\text{NEMA}}+ \\ 0.5\bar{r}_{(r,s),\text{NT}}^{\text{NEMA}} - g_{(r,s),\text{SL}}^{\text{NEMA}}\end{array}\right), \\ g_{(r,s),\text{SL}}^{\text{NEMA}} > \bar{g}_{(p,q),\text{EL}}^{\text{NEMA}} \end{cases}, \quad (23)$$

$$\Omega_{(p,q),(r,s)}^{\text{NEMA,ES}} = \begin{cases} \sum_{h}^{1,4,5,8}\left(2y_{(r,s),h}^{(p,q)} - z_{(r,s),h}^{(p,q)}\right)\left(\begin{array}{l}0.5\bar{r}_{(p,q),\text{ET}}^{\text{NEMA}}- \\ 0.5r_{(r,s),\text{ST}}^{\text{NEMA}} + \bar{g}_{(p,q),\text{ET}}^{\text{NEMA}}\end{array}\right) \\ \quad + \sum_{h}^{2,3,6,7}\left(z_{(r,s),h}^{(p,q)} - 2y_{(r,s),h}^{(p,q)}\right)\left(\begin{array}{l}0.5\bar{r}_{(p,q),\text{ET}}^{\text{NEMA}}+ \\ 0.5r_{(r,s),\text{ST}}^{\text{NEMA}} - \bar{g}_{(r,s),\text{NL}}^{\text{NEMA}}\end{array}\right), \\ g_{(p,q),\text{WL}}^{\text{NEMA}} \le \bar{g}_{(r,s),\text{NL}}^{\text{NEMA}} \\ \sum_{h}^{1,4,5,8}\left(2y_{(r,s),h}^{(p,q)} - z_{(r,s),h}^{(p,q)}\right)\left(\begin{array}{l}0.5\bar{r}_{(p,q),\text{ET}}^{\text{NEMA}}- \\ 0.5r_{(r,s),\text{ST}}^{\text{NEMA}} + \bar{g}_{(p,q),\text{ET}}^{\text{NEMA}}\end{array}\right) \\ \quad + \sum_{h}^{2,3,6,7}\left(2y_{(r,s),h}^{(p,q)} - z_{(r,s),h}^{(p,q)}\right)\left(\begin{array}{l}0.5\bar{r}_{(p,q),\text{ET}}^{\text{NEMA}}+ \\ 0.5r_{(r,s),\text{ST}}^{\text{NEMA}} - \bar{g}_{(p,q),\text{WL}}^{\text{NEMA}}\end{array}\right), \\ g_{(p,q),\text{WL}}^{\text{NEMA}} > \bar{g}_{(r,s),\text{NL}}^{\text{NEMA}} \end{cases}. \quad (24)$$

The 0/1 variables in (19)–(24) should further satisfy the following constraints to exclude the ineligible 0/1 combinations:

$$\left.\begin{array}{l}\sum_{h=1}^{8} z_{(r,s),h}^{(p,q)} = 1 \\ z_{(r,s),h}^{(p,q)} - y_{(r,s),h}^{(p,q)} \ge 0, \forall h \le 8\end{array}\right\}. \quad (25)$$

Table 5 shows how the introduced 0/1 variables select the optimal phase sequence at an intersection of Type II under the NEMA phasing.

As illustrated in Fig. 1, there are four different phase sequences for both the W-E and S-N directions under the NEMA phasing, which leads to 16 different phase sequences at an intersection of Type II. The 16 different phase sequences are shown in Table 5. The first and second numbers in parenthesis in Table 5 represent the number of the phase sequence in Fig. 1(a) and (b), respectively.

TABLE 5. Relationships between 0/1 variables and phase sequences in NEMA phasing for an intersection of type II.

Phase sequences	h	$z_{(r,s),h}^{(p,q)}$	$y_{(r,s),h}^{(p,q)}$
(1, 1)	1	1	0
(1, 2)	2	1	0
(1, 3)	3	1	0
(1, 4)	4	1	0
(2, 1)	2	1	1
(2, 2)	1	1	1
(2, 3)	4	1	1
(2, 4)	3	1	1
(3, 1)	5	1	0
(3, 2)	6	1	0
(3, 3)	7	1	0
(3, 4)	8	1	0
(4, 1)	6	1	1
(4, 2)	5	1	1
(4, 3)	8	1	1
(4, 4)	7	1	1

D) General Formulas for $\Delta_{(p,q)}^{Split}$, $\Delta_{(r,s)}^{Split}$ and Ω for Intersection of Type II: Similarly, when the split phasing is used, the optimal phase sequences of an intersection of Type II are determined concurrently by $\Delta_{(p,q)}^{\text{Split}}$, $\Delta_{(r,s)}^{\text{Split}}$ and Ω. Their general formulas can be expressed by

$$\Delta_{(p,q)}^{\text{Split}} = \begin{cases} \sum_{h=1}^{3}\left(v_{(r,s),h}^{(p,q)} - 0.5u_{(r,s),h}^{(p,q)}\right)\left(g_{(p,q),\text{WT}}^{\text{Split}} + \overline{g}_{(p,q),\text{ET}}^{\text{Split}}\right) \\ \quad + \left(2v_{(r,s),3}^{(p,q)} - u_{(r,s),3}^{(p,q)}\right)\overline{g}_{(r,s),\text{NT}}^{\text{Split}}, g_{(r,s),\text{ST}}^{\text{Split}} \geq \overline{g}_{(r,s),\text{NT}}^{\text{Split}} \\ \left[\begin{array}{l}\sum_{h=1}^{2}\left(v_{(r,s),h}^{(p,q)} - 0.5u_{(r,s),h}^{(p,q)}\right) \\ \quad + \left(0.5u_{(r,s),3}^{(p,q)} - v_{(r,s),3}^{(p,q)}\right)\end{array}\right]\left(g_{(p,q),\text{WT}}^{\text{Split}} + \overline{g}_{(p,q),\text{ET}}^{\text{Split}}\right) \\ \quad + \left(u_{(r,s),3}^{(p,q)} - 2v_{(r,s),3}^{(p,q)}\right)g_{(r,s),\text{ST}}^{\text{Split}}, g_{(r,s),\text{ST}}^{\text{Split}} < \overline{g}_{(r,s),\text{NT}}^{\text{Split}} \end{cases}, \tag{26}$$

$$\Delta_{(r,s)}^{\text{Split}} = \begin{cases} \sum_{h=1}^{3}(-1)^{h+1}\left(v_{(r,s),h}^{(p,q)} - 0.5u_{(r,s),h}^{(p,q)}\right)\left(g_{(r,s),\text{ST}}^{\text{Split}} + \overline{g}_{(r,s),\text{NT}}^{\text{Split}}\right) \\ \quad + \left(2v_{(r,s),3}^{(p,q)} - u_{(r,s),3}^{(p,q)}\right)g_{(p,q),\text{WT}}^{\text{Split}}, \overline{g}_{(p,q),\text{ET}}^{\text{Split}} \geq g_{(p,q),\text{WT}}^{\text{Split}} \\ \left[\begin{array}{l}\left(v_{(r,s),1}^{(p,q)} - 0.5u_{(r,s),1}^{(p,q)}\right) \\ \quad + \sum_{h=2}^{3}\left(0.5u_{(r,s),h}^{(p,q)} - v_{(r,s),h}^{(p,q)}\right)\end{array}\right]\left(g_{(r,s),\text{ST}}^{\text{Split}} + \overline{g}_{(r,s),\text{NT}}^{\text{Split}}\right) \\ \quad + \left(u_{(r,s),3}^{(p,q)} - 2v_{(r,s),3}^{(p,q)}\right)\overline{g}_{(p,q),\text{ET}}^{\text{Split}}, \overline{g}_{(p,q),\text{ET}}^{\text{Split}} < g_{(p,q),\text{WT}}^{\text{Split}} \end{cases}. \tag{27}$$

The general formulas for $\Omega_{(p,q),(r,s)}^{\text{Split,SW}}$, $\Omega_{(p,q),(r,s)}^{\text{Split,WN}}$, $\Omega_{(p,q),(r,s)}^{\text{Split,NE}}$, and $\Omega_{(p,q),(r,s)}^{\text{Split,ES}}$ for an intersection of Type II can be expressed, respectively, by

$$\Omega_{(p,q),(r,s)}^{\text{Split,SW}} = \begin{cases} \sum_{h=1}^{3}\left(v_{(r,s),h}^{(p,q)} - 0.5u_{(r,s),h}^{(p,q)}\right)\left(g_{(r,s),\text{ST}}^{\text{Split}} + g_{(p,q),\text{WT}}^{\text{Split}}\right) \\ \quad + \left(2v_{(r,s),1}^{(p,q)} - u_{(r,s),1}^{(p,q)}\right)\overline{g}_{(r,s),\text{NT}}^{\text{Split}}, \overline{g}_{(p,q),\text{ET}}^{\text{Split}} \geq \overline{g}_{(r,s),\text{NT}}^{\text{Split}} \\ \left[\begin{array}{l}\left(0.5u_{(r,s),1}^{(p,q)} - v_{(r,s),1}^{(p,q)}\right) \\ \quad + \sum_{h=2}^{3}\left(v_{(r,s),h}^{(p,q)} - 0.5u_{(r,s),h}^{(p,q)}\right)\end{array}\right]\left(g_{(r,s),\text{ST}}^{\text{Split}} + g_{(p,q),\text{WT}}^{\text{Split}}\right) \\ \quad + \left(u_{(r,s),1}^{(p,q)} - 2v_{(r,s),1}^{(p,q)}\right)\overline{g}_{(p,q),\text{ET}}^{\text{Split}}, \overline{g}_{(p,q),\text{ET}}^{\text{Split}} < \overline{g}_{(r,s),\text{NT}}^{\text{Split}} \end{cases}, \tag{28}$$

$$\Omega_{(p,q),(r,s)}^{\text{Split,WN}} = \begin{cases} \left[\begin{array}{l}\left(0.5u_{(r,s),1}^{(p,q)} - v_{(r,s),1}^{(p,q)}\right) \\ \quad + \sum_{h=2}^{3}\left(v_{(r,s),h}^{(p,q)} - 0.5u_{(r,s),h}^{(p,q)}\right)\end{array}\right]\left(g_{(p,q),\text{WT}}^{\text{Split}} + \overline{g}_{(r,s),\text{NT}}^{\text{Split}}\right) \\ \quad + \left(2v_{(r,s),2}^{(p,q)} - u_{(r,s),2}^{(p,q)}\right)\overline{g}_{(p,q),\text{ET}}^{\text{Split}}, g_{(r,s),\text{ST}}^{\text{Split}} \geq \overline{g}_{(p,q),\text{ET}}^{\text{Split}} \\ \left[\begin{array}{l}\sum_{h=1}^{2}\left(0.5u_{(r,s),h}^{(p,q)} - v_{(r,s),h}^{(p,q)}\right) \\ \quad + \left(v_{(r,s),3}^{(p,q)} - 0.5u_{(r,s),3}^{(p,q)}\right)\end{array}\right]\left(g_{(p,q),\text{WT}}^{\text{Split}} + \overline{g}_{(r,s),\text{NT}}^{\text{Split}}\right) \\ \quad + \left(u_{(r,s),2}^{(p,q)} - 2v_{(r,s),2}^{(p,q)}\right)g_{(r,s),\text{ST}}^{\text{Split}}, g_{(r,s),\text{ST}}^{\text{Split}} < \overline{g}_{(p,q),\text{ET}}^{\text{Split}} \end{cases}, \tag{29}$$

$$\Omega_{(p,q),(r,s)}^{\text{Split,NE}} = \begin{cases} \sum_{h=1}^{3}(-1)^{h+1}\left(v_{(r,s),h}^{(p,q)} - 0.5u_{(r,s),h}^{(p,q)}\right)\left(\overline{g}_{(r,s),\text{NT}}^{\text{Split}} + \overline{g}_{(p,q),\text{ET}}^{\text{Split}}\right) \\ \quad + \left(2v_{(r,s),1}^{(p,q)} - u_{(r,s),1}^{(p,q)}\right)g_{(p,q),\text{WT}}^{\text{Split}}, g_{(r,s),\text{ST}}^{\text{Split}} \geq g_{(p,q),\text{WT}}^{\text{Split}} \\ \left[\begin{array}{l}\sum_{h=1}^{2}\left(0.5u_{(r,s),h}^{(p,q)} - v_{(r,s),h}^{(p,q)}\right) \\ \quad + \left(v_{(r,s),3}^{(p,q)} - 0.5u_{(r,s),3}^{(p,q)}\right)\end{array}\right]\left(\overline{g}_{(r,s),\text{NT}}^{\text{Split}} + \overline{g}_{(p,q),\text{ET}}^{\text{Split}}\right) \\ \quad + \left(u_{(r,s),1}^{(p,q)} - 2v_{(r,s),1}^{(p,q)}\right)g_{(r,s),\text{ST}}^{\text{Split}}, g_{(r,s),\text{ST}}^{\text{Split}} < g_{(p,q),\text{WT}}^{\text{Split}} \end{cases}, \tag{30}$$

$$\Omega_{(p,q),(r,s)}^{\text{Split,ES}} = \begin{cases} \sum_{h=1}^{3}(-1)^{h+1}\left(v_{(r,s),h}^{(p,q)} - 0.5u_{(r,s),h}^{(p,q)}\right)\left(\overline{g}_{(p,q),\text{ET}}^{\text{Split}} + g_{(r,s),\text{ST}}^{\text{Split}}\right) \\ \quad + \left(u_{(r,s),2}^{(p,q)} - 2v_{(r,s),2}^{(p,q)}\right)g_{(p,q),\text{WT}}^{\text{Split}}, \overline{g}_{(r,s),\text{NT}}^{\text{Split}} \geq g_{(p,q),\text{WT}}^{\text{Split}} \\ \sum_{h=1}^{3}\left(v_{(r,s),h}^{(p,q)} - 0.5u_{(r,s),h}^{(p,q)}\right)\left(\overline{g}_{(p,q),\text{ET}}^{\text{Split}} + g_{(r,s),\text{ST}}^{\text{Split}}\right) \\ \quad + \left(2v_{(r,s),2}^{(p,q)} - u_{(r,s),2}^{(p,q)}\right)\overline{g}_{(r,s),\text{NT}}^{\text{Split}}, \overline{g}_{(r,s),\text{NT}}^{\text{Split}} < g_{(p,q),\text{WT}}^{\text{Split}} \end{cases}. \tag{31}$$

The 0/1 variables in (26)–(31) should satisfy the following constraints to exclude the ineligible 0/1 combinations:

$$\left.\begin{array}{l}\sum_{h=1}^{3} u_{(r,s),h}^{(p,q)} = 1 \\ u_{(r,s),h}^{(p,q)} - v_{(r,s),h}^{(p,q)} \geq 0, \forall h \leq 3\end{array}\right\}. \tag{32}$$

TABLE 6. Relationships between 0/1 variables and phase sequences in split phasing for an intersection of type II.

Phase sequence	h	$u_{(r,s),h}^{(p,q)}$	$v_{(r,s),h}^{(p,q)}$
1	1	1	0
2	2	1	0
3	3	1	1
4	2	1	1
5	3	1	0
6	1	1	1

Table 6 shows how the phase sequences in the split phasing are represented by the 0/1 variables for an intersection of Type II.

E) General Formulas for $\Delta_{(p,q)}^{NEMA}$ and $\Delta_{(r,s)}^{NEMA}$ for Intersection of Type III: The general formulas for $\Delta_{(p,q)}^{\text{NEMA}}$ and $\Delta_{(r,s)}^{\text{NEMA}}$ for an intersection of Type III are the same as those in (13) and (14), respectively.

F) General Formulas for $\Delta_{(p,q)}^{Split}$ and $\Delta_{(r,s)}^{Split}$ for Intersection of III: According to Table 3, the general formulas for $\Delta_{(p,q)}^{\text{Split}}$ and $\Delta_{(r,s)}^{\text{Split}}$ for an intersection of Type III are:

$$\Delta_{(p,q)}^{\text{Split}} = \begin{cases} \sum_{h=1}^{2} \left(v_{(p,q),h} - 0.5u_{(p,q),h}\right)\left(g_{(p,q),\text{WT}}^{\text{Split}} + \bar{g}_{(p,q),\text{ET}}^{\text{Split}}\right) \\ \quad + \left(2v_{(p,q),2} - u_{(p,q),2}\right)\bar{g}_{(p,q),\text{NT}}^{\text{Split}},\ g_{(p,q),\text{ST}}^{\text{Split}} \geq \bar{g}_{(p,q),\text{NT}}^{\text{Split}} \\ \sum_{h=1}^{2} (-1)^{h+1}\left(v_{(p,q),h} - 0.5u_{(p,q),h}\right)\left(g_{(p,q),\text{WT}}^{\text{Split}} + \bar{g}_{(p,q),\text{ET}}^{\text{Split}}\right) \\ \quad + \left(u_{(p,q),2} - 2v_{(p,q),2}\right)g_{(p,q),\text{ST}}^{\text{Split}},\ g_{(p,q),\text{ST}}^{\text{Split}} < \bar{g}_{(p,q),\text{NT}}^{\text{Split}} \end{cases}, \tag{33}$$

where

$$\left.\begin{aligned} &\sum_{h=1}^{2} u_{(p,q),h} = 1 \\ &u_{(p,q),h} - v_{(p,q),h} \geq 0, \forall h \leq 2 \end{aligned}\right\}, \tag{34}$$

$$\Delta_{(r,s)}^{\text{Split}} = \begin{cases} \sum_{h=1}^{2} \left(v_{(r,s),h} - 0.5u_{(r,s),h}\right)\left(g_{(r,s),\text{ST}}^{\text{Split}} + \bar{g}_{(r,s),\text{NT}}^{\text{Split}}\right) \\ \quad + \left(2v_{(r,s),2} - u_{(r,s),2}\right)g_{(r,s),\text{WT}}^{\text{Split}},\ \bar{g}_{(r,s),\text{ET}}^{\text{Split}} \geq g_{(r,s),\text{WT}}^{\text{Split}} \\ \sum_{h=1}^{2} (-1)^{h+1}\left(v_{(r,s),h} - 0.5u_{(r,s),h}\right)\left(g_{(r,s),\text{ST}}^{\text{Split}} + \bar{g}_{(r,s),\text{NT}}^{\text{Split}}\right) \\ \quad + \left(u_{(r,s),2} - 2v_{(r,s),2}\right)\bar{g}_{(r,s),\text{ET}}^{\text{Split}},\ \bar{g}_{(r,s),\text{ET}}^{\text{Split}} < g_{(r,s),\text{WT}}^{\text{Split}} \end{cases}, \tag{35}$$

and

$$\left.\begin{aligned} &\sum_{h=1}^{2} u_{(r,s),h} = 1 \\ &u_{(r,s),h} - v_{(r,s),h} \geq 0, \forall h \leq 2 \end{aligned}\right\}. \tag{36}$$

Table 7 shows how the phase sequences in the split phasing are represented by the 0/1 variables for an intersection of Type III. As shown in Table 7, some two different phase sequences share the same 0/1 variables, which indicates that the two phase sequences are equivalent in terms of bandwidth maximization.

TABLE 7. Relationships between 0/1 variables and phase sequences in split phasing for an intersection of type III.

Phase sequence	W-E coordinated phase				N-S coordinated phase			
	$u_{(p,q),1}$	$u_{(p,q),2}$	$v_{(p,q),1}$	$v_{(p,q),2}$	$u_{(r,s),1}$	$u_{(r,s),2}$	$v_{(r,s),1}$	$v_{(r,s),2}$
1	1	0	0	/	1	0	0	/
2	1	0	0	/	1	0	1	/
3	0	1	/	1	0	1	/	1
4	1	0	1	/	1	0	0	/
5	0	1	/	0	0	1	/	0
6	1	0	1	/	1	0	1	/

7) *Common Cycle Time Constraints:* If all the intersections in the traffic network operate with the split phasing, the common cycle time constraint can be expressed by

$$\frac{1}{C_{\max}^{\text{Split}}} \leq z \leq \frac{1}{C_{\min}^{\text{Split}}}. \tag{37}$$

where $C_{\min}^{\text{Split}}$ and $C_{\max}^{\text{Split}}$ are the lower and upper limits on the common cycle time when the split phasing is used, and z represents the reciprocal of the common cycle time.

If some intersections in the traffic network operate with the NEMA phasing and the other ones operate with the split phasing, the common cycle time constraint can be expressed by

$$\frac{1}{\min\left\{C_{\max}^{\text{NEMA}}, C_{\max}^{\text{Split}}\right\}} \leq z \leq \frac{1}{\max\left\{C_{\min}^{\text{NEMA}}, C_{\min}^{\text{Split}}\right\}}. \tag{38}$$

where $C_{\min}^{\text{NEMA}}$and $C_{\max}^{\text{NEMA}}$are the lower and upper limits on the common cycle time when the NEMA phasing is used.

In summary, different bandwidth maximization models can be established by combining the developed objective function and constraints. Specifically, Models 1 and 2 can, respectively, maximize the bandwidth in the split and mixed phasing schemes for closed traffic networks. The same maximization for unclosed and mixed traffic networks can be achieved by Models 3 and 4 and Models 5 and 6, respectively. Models 1–6 can be summarized as follows:

Model 1: (1), (2)
s.t. (3)–(6), (10), (12), (26)–(32), (37);
Model 2: (1), (2)
s.t. (3)–(6), (10), (12), (19)–(32), (38);
Model 3: (1), (2)
s.t. (3)–(6), (10), (15)–(18), (33)–(37);
Model 4: (1), (2)
s.t. (3)–(6), (10), (13)–(18), (33)–(36), (38);
Model 5: (1), (2)
s.t. (3)–(6), (10), (12), (15)–(18), (26)–(37);
Model 6: (1), (2)
s.t. (3)–(6), (10), (12)–(36), (38).

The objective function and constraints in Models 1–6 are linear, and some decision variables are required to be integers; thus, Models 1–6 are mixed-integer linear programming problems. Note that we consider the most common situations while summarizing Models 5 and 6. Specifically, there can be no intersections of Type I in the mixed traffic networks. If this occurs, the phase sequence constraints (15)–(18) in Model 5 and (13)–(18) in Model 6 should be removed.

C. MODEL SOLUTION

As stated before, the proposed Models 1–6 are formulated as mixed-integer linear programming problems and can be solved by the branch-and-bound algorithm. Common optimization software, such as Linear Interactive and General Optimizer (LINGO), has the built-in branch-and-bound algorithm to solve mixed-integer linear programming problems. Therefore, the proposed Models 1–6 can be solved by LINGO software, and there is no need to develop a customized algorithm to solve the proposed models.

V. NUMERICAL EXAMPLE

In this section, three different cases (referred to as Cases I, II, and III) were designed, and each case had two test scenarios. The six test scenarios are referred to as Tests 1, 2, 3, 4, 5, and 6, which were used to verify Models 1, 2, 3, 4, 5, and 6, respectively. The optimization software LINGO was used to solve the presented models to yield the coordination plan for each test. The optimization software ran on a laptop computer with a 2.6GHz i7-10750H CPU, 16GB of RAM, and the 64-bit Windows 10 operating system.

A. BASIC PARAMETERS

The test traffic networks in Cases I, II, and III were closed, unclosed, and mixed networks, respectively, and they are illustrated in Fig. 7(a), (b), and (c). For simplicity, a part of the closed traffic network and the whole unclosed traffic network were extracted from the mixed traffic network, which means some intersections in the three traffic networks shared the same basic parameters. The traffic volume for each movement at each intersection is shown in Table 8. Symbols LT, TH, and RT in Table 8 represent the left-turn, through, and right-turn movements, respectively. There were three lanes on each approach at each intersection. The lane near the road centerline was divided into an exclusive left-turn lane and a shared left-through lane under conditions in which the intersection operated with the NEMA and the split phasing. The remaining two lanes were divided into a through lane and an exclusive right-turn lane, respectively, regardless of which phasing schemes were adopted. When the mixed phasing scheme was used in the traffic networks, intersections operating with the split phasing are listed as follows: (1, 2), (1, 4), (2, 1), (8, 2), and (8, 3) in Case I; (1, 2), (1, 4), (3, 2), (3, 4), (4, 2), and (5, 3) in Case II; and (1, 2), (1, 4), (2, 1), (3, 2), (3, 4), and (4, 2) in Case III. It was assumed that the outbound and inbound link distances were the same, as were the progression speeds. Furthermore, it was assumed that there are no initial queues on all links. The link distances are shown in Fig. 7, and the progression

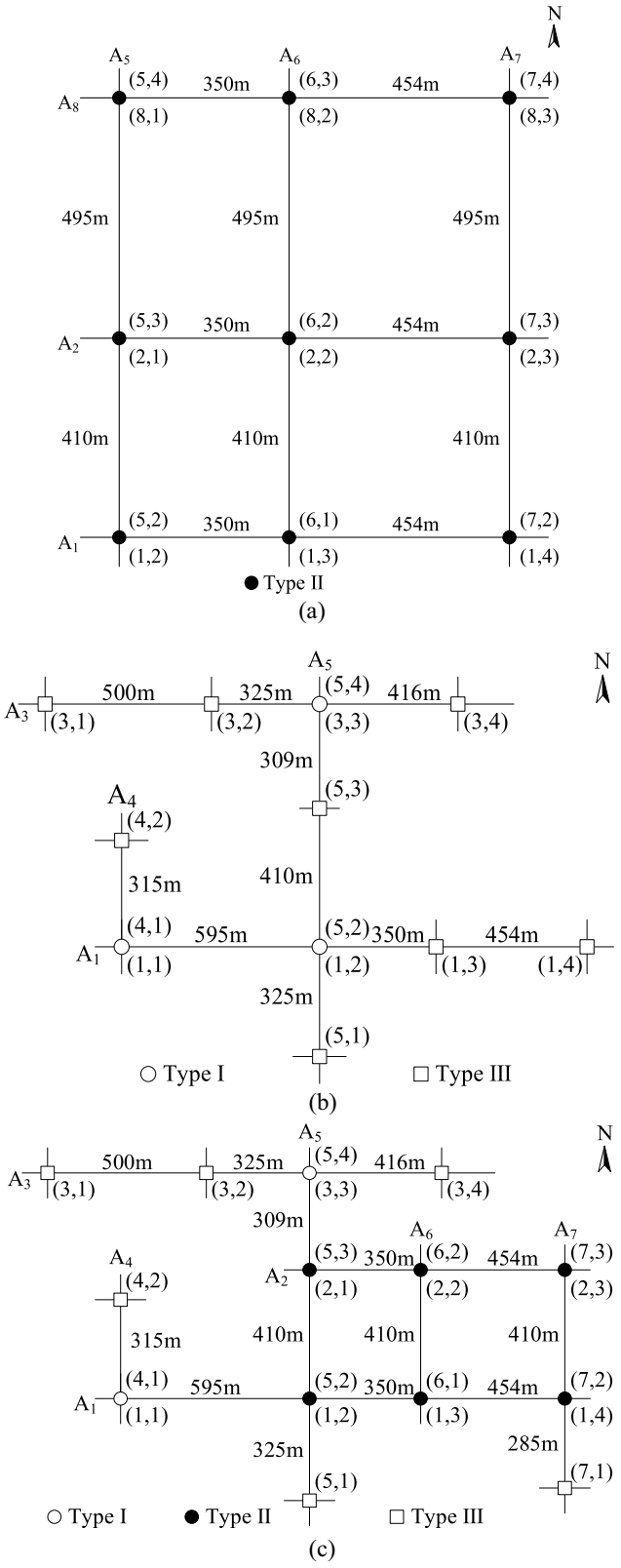

FIGURE 7. Test traffic networks. (a) Case I. (b) Case II. (c) Case III.

TABLE 8. Traffic volumes at each intersection (pcu/h).

Intersection	West			East			South			North		
	LT	TH	RT	LT	TH	RT	LT	TH	RT	LT	TH	RT
(1, 1), (4, 1)	255	391	232	302	427	210	350	485	220	258	400	234
(1, 2), (5, 2)	276	372	221	318	404	238	320	414	215	348	462	215
(1, 3), (6, 1)	276	400	259	324	440	248	280	418	218	339	410	240
(1, 4), (7, 2)	294	426	237	354	402	259	346	386	240	310	354	264
(2, 1), (5, 3)	304	336	227	350	391	208	312	397	219	357	448	299
(2, 2), (6, 2)	305	363	244	310	405	215	320	390	232	357	435	224
(2, 3), (7, 3)	352	380	220	321	390	220	330	394	215	344	387	210
(3, 1)	307	376	217	312	392	223	321	430	276	340	392	205
(3, 2)	332	445	215	279	415	224	255	377	217	324	445	257
(3, 3), (5, 4)	290	386	310	334	428	206	264	420	225	322	460	226
(3, 4)	313	406	214	355	447	215	317	424	213	254	362	204
(4, 2)	310	405	228	334	450	234	365	375	210	325	330	216
(5, 1)	335	386	205	314	368	211	302	403	228	335	453	213
(7, 1)	347	430	225	336	409	230	302	395	216	315	362	268
(8, 1), (5, 4)	251	355	285	346	414	240	306	387	216	382	473	227
(8, 2), (6, 3)	307	360	286	350	465	203	303	402	205	305	380	232
(8, 3), (7, 4)	309	355	206	345	412	236	364	385	217	318	390	242

TABLE 9. Green time information at each intersection (cycles).

Intersection	West		East		South		North	
	LT	TH	LT	TH	LT	TH	LT	TH
(1, 1), (4, 1)	0.17957, 0.22524	0.27096, 0.22524	0.20929, 0.25419	0.30068, 0.25419	0.24255, 0.29114	0.33927, 0.29114	0.18048, 0.22943	0.27720, 0.22943
(1, 2), (5, 2)	0.19026, 0.22237	0.25272, 0.22237	0.21603, 0.24777	0.27849, 0.24777	0.21739, 0.25189	0.28863, 0.25189	0.24262, 0.27797	0.31386, 0.27797
(1, 3), (6, 1)	0.18844, 0.23415	0.27009, 0.23415	0.21877, 0.26464	0.30042, 0.26464	0.20742, 0.24177	0.28224, 0.24177	0.22890, 0.25944	0.30372, 0.25944
(1, 4), (7, 2)	0.22262, 0.25070	0.28784, 0.25070	0.23919, 0.26323	0.30441, 0.26323	0.23378, 0.25487	0.26231, 0.25487	0.21066, 0.23120	0.23919, 0.23120
(2, 1), (5, 3)	0.20894, 0.22107	0.23396, 0.22107	0.24371, 0.25596	0.26873, 0.25596	0.21443, 0.24490	0.27502, 0.24490	0.24731, 0.27807	0.30790, 0.27807
(2, 2), (6, 2)	0.20819, 0.23154	0.26140, 0.23154	0.22324, 0.24784	0.27645, 0.24784	0.21843, 0.24610	0.26906, 0.24610	0.24630, 0.27452	0.29693, 0.27452
(2, 3), (7, 3)	0.23784, 0.25259	0.27177, 0.25259	0.22958, 0.24534	0.26351, 0.24534	0.22950, 0.24983	0.26622, 0.24983	0.23243, 0.25224	0.26915, 0.25224
(3, 1)	0.20898, 0.23798	0.26005, 0.23798	0.21578, 0.24530	0.26685, 0.24530	0.23599, 0.26167	0.29272, 0.26167	0.23145, 0.25505	0.28818, 0.25505
(3, 2)	0.27054	0.27054	0.24164	0.24164	0.22006	0.22006	0.26776	0.26776
(3, 3), (5, 4)	0.19891, 0.23278	0.26402, 0.23278	0.22846, 0.26240	0.29357, 0.26240	0.18506, 0.23554	0.28728, 0.23554	0.22024, 0.26928	0.32246, 0.26928
(3, 4)	0.24983	0.24983	0.27866	0.27866	0.25747	0.25747	0.21404	0.21404
(4, 2)	0.24706	0.24706	0.27091	0.27091	0.25570	0.25570	0.22633	0.22633
(5, 1)	0.22977, 0.24896	0.26588, 0.24896	0.21629, 0.23550	0.25240, 0.23550	0.20713, 0.24344	0.28277, 0.24344	0.23506, 0.27210	0.31070, 0.27210
(7, 1)	0.23820, 0.26830	0.29133, 0.26830	0.22764, 0.25725	0.28077, 0.25725	0.21878, 0.24068	0.26762, 0.24068	0.21341, 0.23377	0.26225, 0.23377
(8, 1), (5, 4)	0.17878, 0.20796	0.23987, 0.20796	0.23378, 0.26081	0.29487, 0.26081	0.20676, 0.23782	0.26489, 0.23782	0.26146, 0.29341	0.31959, 0.29341
(8, 2), (6, 3)	0.20757, 0.23224	0.26466, 0.23224	0.25731, 0.28378	0.31440, 0.28378	0.21207, 0.24547	0.27181, 0.24547	0.20622, 0.23851	0.26596, 0.23851
(8, 3), (7, 4)	0.20949, 0.23072	0.24790, 0.23072	0.24091, 0.26303	0.27932, 0.26303	0.24678, 0.26025	0.27995, 0.26025	0.23124, 0.24600	0.26441, 0.24600

speeds of all the links were set to be 12.5 m/s. The saturation flow rate was assumed to be 1800 pcu/h/lane.

B. MODEL SOLUTIONS

1) *Green Time (in Cycles) Calculation:* The green times for the left-turn and through movements at each intersection were calculated based on the traffic volumes shown in Table 8 and the phasing schemes adopted. The computed results of the green times are shown in Table 9. Note that the first value in a cell in Table 9 is the green time when the NEMA phasing was used, and the second value is the green time when the split phasing was used if there are two values in a cell. Then, the red times (in cycles) for the left-turn and through movements can be easily obtained.

TABLE 10. Lower and upper limits on common cycle time (s).

Phasing scheme	Case I	Case II	Case III
Split phasing scheme	[82, 106]	[82, 105]	[82, 105]
Mixed phasing scheme	[90, 106]	[90, 106]	[90, 106]
NEMA phasing scheme	[90, 118]	-	-

2) *Common Cycle Time Calculation:* The cycle time for an intersection can be computed by:

$$C = \frac{L}{1 - \frac{Y}{X}}, \tag{39}$$

where L is the total lost time, Y is the total ratio of the volume to the saturation flow rate, and X is the v/c ratio. This study assumed L equaled 12 s and that the v/c ratio was in the range of 0.9 to 0.95.

By using (39), the lower and upper limits on the cycle time for an intersection can be easily obtained. Then, the lower limit on the common cycle time was $\max\{C^p_{min,(1,1)}, \ldots, C^p_{min,(M,N_i)}\}$ and the upper limit on it was $\min\{C^p_{max,(1,1)}, \ldots, C^p_{max,(M,N_i)}\}$. Symbol p represents the phasing schemes: the NEMA or the split phasing. $C^p_{min,(i,j)}$ and $C^p_{max,(i,j)}$ are the lower and upper limits for (i, j). Therefore, the lower and upper limits on the common cycle time for traffic networks in Cases I, II and III are shown in Table 10.

3) *Coordination Plan Generation:* The coordination plans of Tests 1, 2, 3, 4, 5, and 6 were generated by Models 1, 2, 3, 4, 5, and 6, respectively, and they are shown in Table 11. According to the LINGO solution reports, it was known that the global optimal solution for each test was found. In terms of computation time, the minimum and maximum computation time were 0.8 s and 212.47 s, respectively, which means that the optimal coordination plan was obtained in less 4 minutes, which was perfectly acceptable. In more detail, the computation time of test 5 was larger than those of the five other tests, which was because it had the largest number of constraints.

The values of the key variables, the bandwidth, sequence, and common cycle time were directly obtained from the LINGO solution reports, and they are shown in Table 11. However, the offset could not be directly obtained. In this study, offset is defined as the time difference between the beginning of the outbound green time at (i, j) and that at $(i, j+1)$. According to the definition, the offset can be computed by $w_{(i,j)} + t_{(i,j),(i,j+1)} - w_{(i,j),(i,j+1)}$, and the computed results are also displayed in Table 11.

The ratios (measured as percentages) of the outbound [inbound] bandwidths obtained from the LINGO solution reports to the outbound [inbound] theoretical bandwidths were computed, and their results are shown in parenthesis in Table 11. The outbound [inbound] theoretical bandwidth is defined as the minimum green time between adjacent intersections in the outbound [inbound]. As shown in Table 11, the ratios greater than or equal to 80% in Tests 1, 2, 3, 4, 5, and 6 accounted for 83.3%, 100.0%, 90.0%, 100.0%, 90.0%, and 93.3%, respectively.

C. CORRECTNESS VERIFICATION

The correctness of Models 1–6 was verified by using the time–space diagram. The principle of the correctness verification is described as follows.

Based on the values of $b_{(i,j),(i,j+1)}$, $\overline{b}_{(i,j),(i,j+1)}$, $w_{(i,j)}$, $w_{(i,j),(i,j+1)}$, $\overline{w}_{(i,j),(i,j+1)}$, $t_{(i,j),(i,j+1)}$, and $\overline{t}_{(i,j),(i,j+1)}$, the phase sequences, the common cycle times from the LINGO solution reports, as well as the green time information from Table 9, we can also display the coordination plans in the format of a time–space diagram. One can see that the fourth interference variable $\overline{w}_{(i,j+1)}$ was not used in the process of drawing the time–space diagram. This was because that the three interference variables, namely $w_{(i,j)}$, $\overline{w}_{(i,j),(i,j+1)}$, and $w_{(i,j),(i,j+1)}$ were sufficient to finish the time–space diagram. In other words, a new fourth interference variable can be obtained from the time–space diagram, and it is denoted as $\overline{w}^{\text{Draw}}_{(i,j+1)}$. $\overline{w}^{\text{Draw}}_{(i,j+1)}$ is defined as the time from the left side of the inbound red time at $(i, j+1)$ to the right side of the corresponding inbound bandwidth. $\overline{w}^{\text{Draw}}_{(i,j+1)}$ is positive if the right side of the inbound bandwidth is to the left of the left side of the inbound red time, otherwise it is negative. At this point, there were two different values for the fourth interference variable: one was $\overline{w}^{\text{Draw}}_{(i,j+1)}$ obtained from the time–space diagram, and the other was the theoretical value $\overline{w}_{(i,j+1)}$ obtained from the LINGO solution report. Therefore, it is natural to think that the absolute difference between $\overline{w}^{\text{Draw}}_{(i,j+1)}$ and $\overline{w}_{(i,j+1)}$ can be a new index to verify the correctness of Models 1–6. The results of the new index are shown in Table 12. Notice that the time–space diagrams in this study were drawn using the Microsoft Visio software. Four digits after the decimal point can be retained in the software, which can fully satisfy the precision requirements for correctness verification. Additionally note that, for simplicity, the bandwidths were rounded to one decimal place in Table 11. However, they were rounded to four decimal places while drawing the time–space diagrams to ensure the precision. In addition, it is common that the green and red times must be integers, and therefore, they were rounded to zero decimal places while drawing the time–space diagrams.

As shown in Table 12, the minimum and maximum values of the absolute difference were 0 and 0.9697, respectively. It is well known that the increase or decrease in the green (red) time must be integers and are at least 1 s. From this perspective, all the absolute differences were very small, which indicated that all the proposed models are correct. The absolute differences are due to the rounding of the common cycle time, the green time, and the red time.

D. SIMULATION COMPARISON

The traffic simulation software VISSIM was utilized to compare the performance of MULTIBAND-96 and Models 1 and 2. It is worth noting that MULTIBAND-96 mainly optimizes bandwidths in closed traffic networks, as do Models 1 and 2.

TABLE 11. (a) Coordination plans for tests 1 and 2 generated by models 1 and 2, respectively. (b) Coordination plans for tests 3 and 4 generated by models 3 and 4, respectively. (c) The coordination plans for tests 5 and 6 generated by models 5 and 6, respectively.

(a)

Intersection	Test 1: Split phasing scheme was used in Case I (Model 1). Computation time was 34.90 s					Test 2: Mixed phasing scheme was used Case I (Model 2) Computation time was 67.91 s.				
	Outbound bandwidth (s)	Inbound bandwidth (s)	Offset (s)	Sequence	Common cycle (s)	Outbound bandwidth (s)	Inbound bandwidth (s)	Offset (s)	Sequence	Common cycle (s)
(1, 2)	-	-	-	1		-	-	-	4	
(1, 3)	18.2(100.0%)	16.5(82.5%)	28	3		23.6(98.3%)	23.8(91.5%)	24	(1, 2)	
(1, 4)	16.7(87.9%)	17.2(78.2%)	39	3		26.6(98.5%)	27.4(97.9%)	38	3	
(2, 1)	-	-	-	5		-	-	-	2	
(2, 2)	17.7(98.3%)	15.5(73.8%)	28	6		23.4(100.0%)	22.5(83.3%)	24	(2, 1)	
(2, 3)	15.2 (80.0%)	14.7(73.5%)	40	6		22.8(81.4%)	23.1(82.5%)	41	(4, 3)	
(8, 1)	-	-	-	5		-	-	-	(3, 4)	
(8, 2)	14.9(87.6%)	17.1(81.4%)	30	6		23.3(93.2%)	26.8(89.3%)	27	5	
(8, 3)	14.5(76.3%)	18.4(83.6%)	41	6	82	20.7(86.3%)	26.7(92.1%)	40	4	106
(5, 2)	-	-	-	1		-	-	-	4	
(5, 3)	20.0(100.0%)	21.7(94.3%)	33	5		22.5(86.5%)	23.5(81.0%)	29	2	
(5, 4)	18.4(92.0%)	21.3(92.6%)	41	5		25.4(97.7%)	29.4(98.0%)	37	(3, 4)	
(6, 1)	-	-	-	3		-	-	-	(1, 2)	
(6, 2)	19.4(97.0%)	20.4(97.1%)	32	6		26.2(90.3%)	27.5(85.9%)	30	(2, 1)	
(6, 3)	20.1(100.0%)	19.6(98.0%)	40	6		26.0(100.0%)	25.3(100.0%)	41	5	
(7, 2)	-	-	-	3		-	-	-	3	
(7, 3)	19.5(97.5%)	17.5(92.1%)	32	6		22.3(82.6%)	20.0(83.3%)	27	(4, 3)	
(7, 4)	19.1(95.5%)	19.2(96.0%)	41	6		27.6(100.0%)	26.1(100.0%)	40	4	

(b)

Intersection	Test 3: Split phasing scheme was used in Case II (Model 3) Computation time was 2.28 s.					Test 4: Mixed phasing scheme was used in Case II (Model 4) Computation time was 0.80 s.				
	Outbound bandwidth (s)	Inbound bandwidth (s)	Offset (s)	Sequence	Common cycle (s)	Outbound bandwidth (s)	Inbound bandwidth (s)	Offset (s)	Sequence	Common cycle (s)
(1, 1)	-	-	-	6		-	-	-	2	
(1, 2)	19.5(84.8%)	22.4(89.6%)	51	4		21.2(100.0%)	23.8(99.2%)	52	4	
(1, 3)	22.9(99.6%)	23.1(92.4%)	27	1 or 2		21.3(100.0%)	21.6(90.0%)	23	1	
(1, 4)	24.1(100.0%)	24.9(92.2%)	36	3		23.8(99.2%)	24.6(98.4%)	36	5	
(3, 1)	-	-	-	3		-	-	-	1	
(3, 2)	24.5(98.0%)	24.8(99.2%)	37	4 or 6		21.7(86.8%)	19.1(83.0%)	36	3	
(3, 3)	24.0(100.0%)	24.9(99.6%)	28	1	103	23.4(93.6%)	23.2(100.0%)	24	3	96
(3, 4)	21.8(90.8%)	22.9(84.8%)	35	3		24.0(100.0%)	25.3(93.7%)	35	1 or 2	
(4, 1)	-	-	-	6		-	-	-	3	
(4, 2)	26.3(100.0%)	23.3(100.0%)	28	1 or 4		24.5(100.0%)	21.7(98.6%)	33	5	
(5, 1)	-	-	-	2 or 6		-	-	-	2	
(5, 2)	24.3(97.2%)	26.6(95.0%)	24	4		24.2(100.0%)	26.5(98.1%)	27	4	
(5, 3)	19.7(78.8%)	22.9(79.0%)	27	2 or 6		20.4(88.7%)	23.8(88.1%)	37	3	
(5, 4)	24.3(100.0%)	25.9(92.5%)	25	1		23.5(100.0%)	25.1(93.0%)	23	3	

(c)

Intersection	Test 5: Split phasing scheme was used in Case III (Model 5). Computation time was 212.47 s.					Test 6: Mixed phasing scheme was used in Case III (Model 6). Computation time was 36.68 s.				
	Outbound bandwidth (s)	Inbound bandwidth (s)	Offset (s)	Sequence	Common cycle (s)	Outbound bandwidth (s)	Inbound bandwidth (s)	Offset (s)	Sequence	Common cycle (s)
(1, 1)	-	-	-	1		-	-	-	2	
(1, 2)	20.5(93.2%)	23.5(97.9%)	49	2		21.3(100.0%)	23.8(99.2%)	52	4	
(1, 3)	21.6(98.2%)	9.4(39.2%)	28	3		21.3(100.0%)	21.6(90.0%)	23	(1, 4)	
(1, 4)	22.7(98.7%)	23.5(90.4%)	35	4		24.1(100.0%)	23.7(94.8%)	36	5	
(2, 1)	-	-	-	4		-	-	-	3	
(2, 2)	21.4(100.0%)	19.0(76.0%)	27	2		18.5(88.1%)	19.6(78.4%)	21	(4, 1)	
(2, 3)	22.5(100.0%)	22.7(98.7%)	35	5		25.1(100.0%)	25.1(100.0%)	36	(1, 2)	
(3, 1)	-	-	-	3		-	-	-	1	
(3, 2)	22.2(96.5%)	19.6(81.7%)	36	4 or 6	97	21.4(85.6%)	18.8(81.7%)	35	3	96
(3, 3)	21.6(93.9%)	23.3(97.1%)	25	2		23.1(92.4%)	23.2(100.0%)	24	3	
(3, 4)	22.4(97.4%)	23.6(94.4%)	34	3		24.0(100.0%)	25.3(93.7%)	34	1 or 2	
(4, 1)	-	-	-	1		-	-	-	3	
(4, 2)	24.8(99.2%)	22.0(100.0%)	25	2 or 6		24.5(100.0%)	21.7(98.6%)	28	5	
(5, 1)	-	-	-	1 or 4		-	-	-	2	
(5, 2)	23.5(97.9%)	25.8(99.2%)	25	2		24.2(100.0%)	26.5(98.1%)	26	4	
(5, 3)	23.8(99.2%)	7.5(27.8%)	33	4		20.6(89.6%)	24.0(88.9%)	36	3	
(5, 4)	22.8(99.1%)	24.4(93.8%)	26	2		23.5(100.0%)	25.1(93.0%)	25	3	
(6, 1)	-	-	-	3		-	-	-	(1, 4)	
(6, 2)	19.5(84.8%)	20.5(82.0%)	37	2		25.8(99.2%)	20.6(73.6%)	34	(4, 1)	
(7, 1)	-	-	-	2 or 6		-	-	-	4	
(7, 2)	21.6(93.9%)	20.3(92.3%)	25	4		23.7(94.8%)	22.2(100.0%)	24	5	
(7, 3)	22.1(92.1%)	19.8(90.0%)	35	5		23.9(95.6%)	21.5(97.7%)	33	(1, 2)	

Therefore, the above three models were compared. The coordination plan for the closed traffic network illustrated in Fig. 7(a), which was yielded by MULTIBAND-96, is shown in Table 13. The measures of effectiveness (MOEs) included the average delay time and the average number of stops. To avoid randomness, each scenario was simulated

TABLE 12. (a) Results of the absolute difference for case I. (b) Results of the absolute difference for case II. (c) Results of the absolute difference for case III.

(a)

Inter-section	Test 1: Split phasing scheme was used in Case I (Model 1)			Test 2: Mixed phasing scheme was used Case I (Model 2)		
	$\bar{w}^{Draw}_{(i,j+1)}$	$\bar{w}_{(i,j+1)}$	AD	$\bar{w}^{Draw}_{(i,j+1)}$	$\bar{w}_{(i,j+1)}$	AD
(1, 3)	-0.1322	0	0.1322	0.1809	0	0.1809
(1, 4)	-0.3157	0	0.3157	0.7813	0.455	0.3263
(2, 2)	-0.0818	0	0.0818	7.725	6.8001	0.9249
(2, 3)	0	0	0	-0.2918	0	0.2918
(8, 2)	0.4987	0	0.4987	3.7054	3.2594	0.446
(8, 3)	0	0	0	-0.0198	0	0.0198
(5, 3)	0.5273	1.0901	0.5628	6.1	5.9348	0.1652
(5, 4)	0.3977	0	0.3977	4.5563	4.4329	0.1234
(6, 2)	1.8665	2.0668	0.2003	4.2573	3.9545	0.3028
(6, 3)	0	0	0	-0.2911	0	0.2911
(7, 3)	2.6097	3.1671	0.5574	8.691	8.4845	0.2065
(7, 4)	-0.0001	0	0.0001	-0.4432	0	0.4432

Note: AD represents the absolute difference

(b)

Inter-section	Test 3: Split phasing scheme was used in Case II (Model 3)			Test 4: Mixed phasing scheme was used Case II (Model 4)		
	$\bar{w}^{Draw}_{(i,j+1)}$	$\bar{w}_{(i,j+1)}$	AD	$\bar{w}^{Draw}_{(i,j+1)}$	$\bar{w}_{(i,j+1)}$	AD
(1, 2)	-0.2634	0	0.2634	0.0749	0	0.0749
(1, 3)	3.5945	4.1248	0.5303	2.4189	2.1721	0.2468
(1, 4)	-0.012	0	0.012	0.3449	0.7168	0.3719
(3, 2)	-0.3537	0.1378	0.4915	3.7237	4.0858	0.3621
(3, 3)	1.9909	2.1383	0.1474	5.099	4.9853	0.1137
(3, 4)	-0.1345	0	0.1345	0.8216	0	0.8216
(4, 2)	-0.7886	0	0.7886	-0.2632	0	0.2632
(5, 2)	2.3396	2.0591	0.2805	0.5595	0	0.5595
(5, 3)	5.0912	5.6972	0.606	0.297	0	0.297
(5, 4)	1.7245	1.8578	0.1333	0.3549	0	0.3549

Note: AD represents the absolute difference

(c)

Inter-section	Test 5: Split phasing scheme was used in Case III (Model 5)			Test 6: Mixed phasing scheme is used Case III (Model 6)		
	$\bar{w}^{Draw}_{(i,j+1)}$	$\bar{w}_{(i,j+1)}$	AD	$\bar{w}^{Draw}_{(i,j+1)}$	$\bar{w}_{(i,j+1)}$	AD
(1, 2)	-0.2789	0	0.2789	-0.6482	0	0.6482
(1, 3)	-0.3366	0	0.3366	2.4189	2.5975	0.1786
(1, 4)	1.2458	1.5489	0.3031	0.64	1.5636	0.9236
(2, 2)	5.3867	4.9925	0.3942	7.4269	6.9089	0.518
(2, 3)	0.7148	1.1188	0.404	-0.9121	0	0.9121
(3, 2)	3.9759	3.867	0.1089	3.4007	4.3704	0.9697
(3, 3)	2.0584	2.1891	0.1307	4.7041	4.9853	0.2812
(3, 4)	0.3315	0	0.3315	0.3161	0	0.3161
(4, 2)	0.4	0	0.4	-0.646	0	0.646
(5, 2)	1.1105	1.2014	0.0909	0.3904	0.2258	0.1646
(5, 3)	19.6	19.4521	0.1479	-0.2013	0	0.2013
(5, 4)	1.3841	1.7495	0.3654	4.0569	4.0774	0.0205
(6, 2)	0.1635	0	0.1635	-0.608	0	0.608
(7, 2)	0.235	0	0.235	0.2441	0	0.2441
(7, 3)	0.8228	0	0.8228	-0.0857	0	0.0857

Note: AD represents the absolute difference

for ten replications using different random seeds. The starting random seed and the increment were set to 42 and 10, respectively. MOEs were obtained by averaging the 10 simulation results and they are summarized in Table 14. The percentages in the parentheses in Table 14 represent the increase or decrease in the MOEs compared with those of the MULTIBAND-96 plans. In detail, Table 14 (a) and (b) shows

TABLE 13. Coordination plans generated by MULTIBAND-96.

NEMA phasing scheme was used in Case I (MULTIBAND-96). Common cycle was 118 s. Computation time was 10.66 s.				
Intersection	Outbound bandwidth (s)	Inbound bandwidth (s)	Offset (s)	Sequence
(1, 2)	-	-	-	(1, 1)
(1, 3)	20.9	21.1	23	(2, 1)
(1, 4)	30.8	31.9	33	(1, 1)
(2, 1)	-	-	-	(1, 2)
(2, 2)	26.8	17.0	27	(2, 2)
(2, 3)	29.4	26.2	34	(1, 2)
(8, 1)	-	-	-	(1, 4)
(8, 2)	24.5	20.5	26	(2, 4)
(8, 3)	23.6	31.0	33	(1, 4)
(5, 2)	-	-	-	(1, 1)
(5, 3)	27.2	31.5	28	(1, 2)
(5, 4)	27.2	31.5	45	(1, 4)
(6, 1)	-	-	-	(2, 1)
(6, 2)	26.2	27.6	29	(2, 2)
(6, 3)	25.5	27.6	46	(2, 4)
(7, 2)	-	-	-	(1, 1)
(7, 3)	24.5	24.6	26	(1, 2)
(7, 4)	24.5	24.6	44	(1, 4)

the average delay time and the average number of stops, respectively, on each link and Table 14 (c) shows the MOEs of the entire traffic network.

From Table 14 (a) and (b), it can be observed that the signal coordination plan generated by Model 1 resulted in smaller average delay time on all links and smaller average number of stops on all links except for the one between intersections (2, 1) and (2, 2). In terms of the MOEs of the entire traffic network, Model 1 plan produced smaller average delay time and smaller average number of stops. When the performance of the Model 2 plan was examined, the average delay time and the average number of stops produced by the Model 2 plan were smaller on some links but larger on other links. At the same time, when checked at the entire traffic network level, the Model 2 plan resulted in larger average delay time but slightly smaller average number of stops. According to the above analysis, one may conclude that Model 1 outperformed MUTIBAND-96, but the same conclusion could not be drawn for Model 2 in terms of the performance measures, which indicated that the split phasing scheme outperformed the existing NEMA phasing scheme in reducing the average delay time and the average number of stops.

VI. CONCLUSION

A group of bandwidth optimization models (referred to as Models 1–6) for split or mixed phasing schemes in different types of traffic networks has been proposed. Specifically, Models 1 and 2 maximized the network bandwidth when the split and mixed phasing schemes were used in closed traffic networks. Models 3 and 4 and Models 5 and 6 achieved the same results in unclosed and mixed traffic networks, respectively. Each model concurrently optimized the phase sequences, offsets and common cycle times. In addition,

TABLE 14. (a) Comparison of average delay time on each link. (b) Comparison of average number of stops on each link. (c) Comparison of MOEs of the entire traffic network.

(a)

Link	Average delay time (s)		
	Model 1	Model 2	MULTIBAND-96
(1, 2)-(1, 3)	20.22(-34.3%)	33.89(10.1%)	30.77
(1, 3)-(1, 4)	19.29(-52.3%)	28.03(-30.7%)	40.45
(2, 1)-(2, 2)	27.81(-11.9%)	30.21(-4.3%)	31.57
(2, 2)-(2, 3)	25.36(-40.8%)	38.68(-9.7%)	42.82
(8, 1)-(8, 2)	23.52(-1.5%)	42.08(76.2%)	23.88
(8, 2)-(8, 3)	23.09(-31.4%)	35.71(6.1%)	33.67
(5, 2)-(5, 3)	26.87(-3.0%)	21.24(-23.3%)	27.71
(5, 3)-(5 4)	29.59(-6.2%)	31.58(0.2%)	31.53
(6, 1)-(6 2)	20.20(-27.2%)	41.70(50.2%)	27.76
(6, 2)-(6, 3)	23.93(-44.2%)	31.38(-26.8%)	42.89
(7, 2)-(7, 3)	21.22(-28.7%)	33.95(14.0%)	29.78
(7, 3)-(7, 4)	23.74(-16.4%)	39.88(40.4%)	28.40

(b)

Link	Average number of stops		
	Model 1	Model 2	MULTIBAND-96
(1, 2)-(1, 3)	0.682(-3.4%)	0.756(7.1%)	0.706
(1, 3)-(1, 4)	0.690(-3.4%)	0.706(-1.1%)	0.714
(2, 1)-(2, 2)	0.749(2.3%)	0.684(-6.6%)	0.732
(2, 2)-(2, 3)	0.690(-1.7%)	0.837(19.2%)	0.702
(8, 1)-(8, 2)	0.654(-5.8%)	0.763(9.9%)	0.694
(8, 2)-(8, 3)	0.662(-2.5%)	0.735(8.2%)	0.679
(5, 2)-(5, 3)	0.657(-1.6%)	0.591(-11.5%)	0.668
(5, 3)-(5 4)	0.648(-13.4%)	0.683(-8.7%)	0.748
(6, 1)-(6 2)	0.578(-12.8%)	0.682(2.9%)	0.663
(6, 2)-(6, 3)	0.654(-25.9%)	0.677(-23.2%)	0.882
(7, 2)-(7, 3)	0.632(-6.1%)	0.710(5.5%)	0.673
(7, 3)-(7, 4)	0.660(-9.7%)	0.767(4.9%)	0.731

(c)

MOEs	Model 1	Model 2	MULTIBAND -96
Average delay time (s)	23.76(-27.2%)	33.97(4.0%)	32.65
Average number of stops	0.663(-7.4%)	0.715(-0.1%)	0.716

Models 1–6 were formulated as mixed-integer linear programming problems and that were solved using the branch-and-bound technique. Finally, we designed three different cases and proposed a new index to verify the correctness of Models 1–6. The results of the new index demonstrated that the proposed models are correct. Furthermore, the simulation results indicated that the split phasing scheme performed better at reducing the average delay time and the average number of stops. In this study, it was assumed that the initial queue clearance times were predetermined, and the corresponding formulas were not presented. Therefore, future studies should focus on deriving the formulas describing the initial queue clearance times.

ACKNOWLEDGMENT

The authors wish to thank Weichen Wang for his help in the process of deriving the formulas for the intranode variables of each phase sequence.

REFERENCES

[1] J. A. Hillier and R. Rothery, "The synchronization of traffic signals for minimum delay," *Transp. Sci.*, vol. 1, no. 2, pp. 81–94, May 1967, doi: 10.1287/trsc.1.2.81.

[2] R. E. Allsop, "Selection of offsets to minimize delay to traffic in a network controlled by fixed-time signals," *Transp. Sci.*, vol. 2, no. 1, pp. 1–13, Feb. 1968, doi: 10.1287/trsc.2.1.1.

[3] Y. J. Lin, H. X. Guan, K. Lu, Y. Y. Ma, and S. J. Zhao, "Eco-oriented signal control of intersections with vehicle type considerations using integrated estimation of driving behavior," *J. Clean. Prod.*, vol. 375, Nov. 2022, Art. no. 133986, doi: 10.1016/j.jclepro.2022.133986.

[4] J. D. C. Little, M. D. Kelson, and N. H. Gartner, "MAXBAND: A program for setting signals on arteries and triangular networks," *Transp. Res. Rec.*, no. 795, pp. 40–46, Dec. 1981.

[5] N. H. Gartner, S. F. Assmann, F. Lasaga, and D. L. Hou, "MULTIBAND-A variable-bandwidth arterial progression scheme," *Transp. Res. Rec. Board*, vol. 1287, pp. 212–222, Jan. 1990.

[6] C. K. Wong and S. C. Wong, "Lane-based optimization of signal timings for isolated junctions," *Transport. Res. B-Meth.*, vol. 37, no. 1, pp. 63–84, Jan. 2003, doi: 10.1016/S0191-2615(01)00045-5.

[7] D. I. Robertson, "TRANSYT: A traffic network study tool," Rd. Res. Lab., Crowthorne, England, Rep. LR-253, Jan. 1969.

[8] C. E. Wallace, K. G. Courage, D. P. Reaves, G.W. Shoene, G.W. Euler, and A. Wilbur, "TRANSYT-7F user's manual," Transpor. Res. Center, Univ. Florida, Gainesville, FL, USA, Rep. UF-TRC-U32 FP-06/07, 1988.

[9] S. Zhang and M. Abdel-Aty, "Real-time pedestrian conflict prediction model at the signal cycle level using machine learning models," *IEEE Open J. Intell. Transp. Syst.*, vol. 3, pp. 176–186, Mar. 2022, doi: 10.1109/OJITS.2022.3155126.

[10] M. Emu, F. B. Kamal, S. Choudhury, and Q. A. Rahman, "Fatality prediction for motor vehicle collisions: Mining big data using deep learning and ensemble methods," *IEEE Open J. Intell. Transp. Syst.*, vol. 3, pp. 199–209, Mar. 2022, doi: 10.1109/OJITS.2022.3160404.

[11] Y. S. Lv, Y. J. Duan, W. W. Kang, Z. X. Li, and F.-Y. Wang, "Traffic flow prediction with big data: a deep learning approach," *IEEE Trans. Intell. Transport. Syst.*, vol. 16, no. 2, pp. 865–873, Apr. 2015, doi: 10.1109/TITS.2014.2345663.

[12] A. J. Huang and S. Agarwal, "Physics-informed deep learning for traffic state estimation: Illustrations with LWR and CTM models," *IEEE Open J. Intell. Transp. Syst.*, vol. 3, pp. 503–518, Jun. 2022, doi: 10.1109/OJITS.2022.3182925.

[13] R. Valiente, B. Toghi, R. Pedarsani, and Y. P. Fallah, "Robustness and adaptability of reinforcement learning-based cooperative autonomous driving in mixed-autonomy traffic," *IEEE Open J. Intell. Transp. Syst.*, vol. 3, pp. 397–410, May 2022, doi: 10.1109/OJITS.2022.3172981.

[14] N. Rajesh, Y. G. Zheng, and B. Shyrokau, "Comfort-oriented motion planning for automated vehicles using deep reinforcement learning," *IEEE Open J. Intell. Transp. Syst.*, vol. 4, pp. 348–359, 2023, doi: 10.1109/OJITS.2023.3275275.

[15] T. Tan, F. Bao, Y. Deng, A. Jin, and Q. H. Dai, "Cooperative deep reinforcement learning for large-scale traffic grid signal control," *IEEE Trans. Cybern.*, vol. 50, no. 6, pp. 2687–2700, Jun. 2020, doi: 10.1109/TCYB.2019.2904742.

[16] J. V. S. Busch, V. Latzko, M. Reisslein, and F. H. P. Fitzek, "Optimised traffic light management through reinforcement learning: traffic state agnostic agent vs. holistic agent with current V2I traffic state knowledge," *IEEE Open J. Intell. Transp. Syst.*, vol. 1, pp. 201–216, Sep. 2020, doi: 10.1109/OJITS.2020.3027518.

[17] H. Wang, H. Chen, Q. Wu, C. B. Ma, and Y. D. Li, "Multi-intersection traffic optimisation: a benchmark dataset and a strong baseline," *IEEE Open J. Intell. Transp. Syst.*, vol. 3, pp. 126–136, Nov. 2021, doi: 10.1109/OJITS.2021.3126126.

[18] W. J. Ma, L. Zou, K. An, N. H. Gartner, and M. Wang, "A partition-enabled multi-mode band approach to arterial traffic signal optimization," *IEEE Trans. Intell. Transport. Syst.*, vol. 20, no. 1, pp. 313–322, Jan. 2019, doi: 10.1109/TITS.2018.2815520.

[19] J. T. Morgan and J. D. C. Little, "Synchronizing traffic signals for maximal bandwidth," *Oper. Res.*, vol. 12, no. 6, pp. 896–912, 1964, doi: 10.1287/opre.12.6.896.

[20] J. D. C. Little, "The synchronization of traffic signals by mixed-integer linear programming," *Oper. Res.*, vol. 14, no. 4, pp. 568–594, 1966, doi: 10.1287/opre.14.4.568.

[21] E. C.-P. Chang, S. L. Cohen, C. Liu, N. A. Chaudhary, and C. Messer, "MAXBAND-86: Program for optimizing left-turn phase sequence in multiarterial closed networks," *Transp. Res. Rec.*, vol. 1181, pp. 61–67, 1988.

[22] C. Stamatiadis and N. H. Gartner, "MULTIBAND-96: A program for variable-bandwidth progression optimization of multiarterial traffic networks," *Transp. Res. Rec.*, vol. 1554, no. 1, pp. 9–17, 1996, doi: 10.1177/0361198196155400102.
[23] N. H. Gartner and C. Stamatiadis, "Arterial-based control of traffic flow in urban grid networks," *Math. Comput. Model.*, vol. 35, nos. 5–6, pp. 657–671, Mar. 2002, doi: 10.1016/S0895-7177(02)80027-9.
[24] C. Zhang, Y. C. Xie, N. H. Gartner, C. Stamatiadis, and T. Arsava, "AM-Band: An asymmetrical multi-band model for arterial traffic signal coordination," *Transp. Res. C: Emerg. Technol.*, vol. 58, pp. 515–531, Sep. 2015, doi: 10.1016/j.trc.2015.04.014.
[25] X. F. Yang, Y. C. Cheng, and G.-L. Chang, "A multi-path progression model for synchronization of arterial traffic signals," *Transp. Res. Part C: Emerg. Technol.*, vol. 53, pp. 93–111, Apr. 2015, doi: 10.1016/j.trc.2015.02.010.
[26] T. Arsava, Y. Xie, and N. H. Gartner, "Arterial progression optimization using OD-BAND: case study and extensions," *Transp. Res. Rec.*, vol. 2558, pp. 1–10, Jan. 2016, doi: 10.3141/2558-01.
[27] B. B. Jing, Y. J. Lin, Y. F. Shou, K. Lu, and J. M. Xu, "Pband: A general signal progression model with phase optimization along urban arterial," *IEEE Trans. Intell. Transport. Syst.*, vol. 23, no. 1, pp. 344–354, Jan. 2022, doi: 10.1109/TITS.2020.3010841.
[28] L. H. Zhang, Z. Q. Song, X. J. Tang, and D. H. Wang, "Signal coordination models for long arterials and grid networks," *Transp. Res. C: Emerg. Technol.*, vol. 71, pp. 215–230, Oct. 2016, doi: 10.1016/j.trc.2016.07.015.
[29] K. Lu, Y. Y. Liu, H. Wu, and J. H. Huang, "Algebraic method of bidirectional green wave coordinated control under asymmetric traffic conditions," *China J. Highw. Transp.*, vol. 28, no. 6, pp. 95–103, Jun. 2015, doi: 10.19721/j.cnki.1001-7372.2015.06.013.
[30] K. Lu, S. Y. Jiang, W. P. Xin, J. H. Zhang, and K. Z. He, "Algebraic method of regional green wave coordinated control," *J. Intell. Transport. Syst.*, vol. 27, no. 6, pp. 799–817, May 2022, doi: 10.1080/15472450.2022.2084335.
[31] H. M. Yan, F. He, X. Lin, J. Y. Yu, M. Li, and Y. H. Wang "Network-level multiband signal coordination scheme based on vehicle trajectory data," *Transp. Res. C: Emerg. Technol.*, vol. 107, pp. 266–286, Oct. 2019, doi: 10.1016/j.trc.2019.08.014.
[32] H. Wang, and D. C. Yao, "Network green-wave band model permitting relaxation of constraints," *China J. Highw. Transp.*, vol. 33, no. 3, pp. 184–194, Mar. 2020, doi: 10.19721/j.cnki.1001-7372.2020.03.016.
[33] K. Lu, J. M. Xu, and Y. S. Li, "Algebraic method of arterial road coordinate control for bidirectional green wave under signal design mode of one-phase-one approach," *China J. Highw. Transp.*, vol. 23, no. 3, pp. 95–101, 2010, doi: 10.19721/j.cnki.1001-7372.2010.03.015.

BINBIN JING received the B.S. degree in traffic engineering from the Shandong University of Technology, Zibo, China, in 2012, and the M.S. degree in transportation engineering and the Ph.D. degree in traffic information engineering and control from the South China University of Technology, Guangzhou, China, in 2015 and 2018, respectively. He is currently a Lecturer with the School of Transportation and Civil Engineering, Nantong University, China. He has chaired one project supported by the National Natural Science Foundation of China and two projects supported by the Jiangsu Education Department. His research interests include traffic signal control and traffic data mining.

QUAN SHI received the Ph.D. degree in management information systems from the University of Shanghai for Science and Technology, Shanghai, China, in 2011. He is currently a Full Professor and the Dean of the School of Transportation and Civil Engineering, Nantong University, Nantong, China. He has chaired two projects supported by the National Natural Science Foundation of China. His research interests include big data analysis in transportation, connected vehicles, and traffic control.

CONG HUANG received the B.S. degree in electrical engineering and automation from Nanjing Forestry University, Nanjing, China, in 2016, and the Ph.D. degree in control science and engineering from Donghua University, Shanghai, China, in 2021. From 2019 to 2020, he was a joint Ph.D. student with the Politecnico di Milano. He is currently a Lecturer with the School of Transportation and Civil Engineering, Nantong University, China. He has chaired one project supported by the Jiangsu Education Department. His research interests include stochastic control and filtering, vehicle platoon control, and estimation for vehicle-borne Li-ion batteries.

PENG PING received the B.S. degree in automation from the Beijing University of Chemical Technology, Beijing, China, in 2010, the M.S. degree in control theory and control engineering from the Nanjing University of Science and Technology, Nanjing, China, in 2013, and the Ph.D. degree in instrument science and technology from Southeast University, Nanjing, in 2020. In 2017, he was a joint Ph.D. student with Nagoya University. He is currently a Lecturer with the School of Transportation and Civil Engineering, Nantong University, China. He has chaired one project supported by the National Natural Science Foundation of China. His research interests include intelligent control theory, traffic information analysis, deep learning, and driving behavior modeling.

YONGJIE LIN (Member, IEEE) received the Ph.D. degree from the School of Control Science and Engineering, Shandong University, China, in 2014. During his Ph.D. program, he has studied with the University of Maryland at College Park, College Park, USA, for one year as a visiting student which was supported by the China Scholarship Council, China. He held a one-year postdoctoral position with the Department of Civil and Environmental Engineering, Northwestern University, USA. He is currently an Associate Professor with the School of Civil Engineering and Transportation, South China University of Technology, China. His research interests include traffic operations and control and traffic data analytics.